



City Research Online

City, University of London Institutional Repository

Citation: Rowane, A. J., Babu, V. M., Rokni, H. B., Moore, J. D., Gavaises, M., Wensing, M., Gupta, A. & McHugh, M. A. (2019). Effect of Composition, Temperature, and Pressure on the Viscosities and Densities of Three Diesel Fuels. *Journal of Chemical & Engineering Data*, 64(12), pp. 5529-5547. doi: 10.1021/acs.jced.9b00652

This is the accepted version of the paper.

This version of the publication may differ from the final published version.

Permanent repository link: <https://openaccess.city.ac.uk/id/eprint/23057/>

Link to published version: <https://doi.org/10.1021/acs.jced.9b00652>

Copyright: City Research Online aims to make research outputs of City, University of London available to a wider audience. Copyright and Moral Rights remain with the author(s) and/or copyright holders. URLs from City Research Online may be freely distributed and linked to.

Reuse: Copies of full items can be used for personal research or study, educational, or not-for-profit purposes without prior permission or charge. Provided that the authors, title and full bibliographic details are credited, a hyperlink and/or URL is given for the original metadata page and the content is not changed in any way.

City Research Online:

<http://openaccess.city.ac.uk/>

publications@city.ac.uk

**Effect of Composition, Temperature, and Pressure on the
Viscosities and Densities of Three Diesel Fuels**

Aaron J. Rowane^{a,b}*, Vikrant Mahesh Babu^c, Houman B. Rokni^{a,b}, Joshua D. Moore^d, Manolis Gavaises^a, Michael Wensing^c, Ashutosh Gupta^d, Mark A. McHugh^e

^a Department of Mechanical Engineering and Aeronautics, City University of London,
Northampton Square, EC1V 0HB London, UK

^b Afton Chemical Limited, London Rd, Bracknell, RG12 2UW, Berkshire, UK

^c Lehrstuhl für Technische Thermodynamik, Friedrich-Alexander Univeristy Erlangen-
Nürnberg, Am Weichselgarten 8, D-91058 Erlangen-Tennenlohe, Germany

^d Afton Chemical Corporation, 500 Spring Street, Richmond, VA, 23219, USA

^e Department of Chemical and Life Science Engineering, Virginia Commonwealth University,
601 W Main St, Richmond, VA, 23284, USA

* Corresponding author; e-mail: aaron.rowane@aftonchemical.com; Phone: +44 1344 304141

Postal Address: Afton Chemical Limited, London Rd, Bracknell, RG12 2UW, Berkshire, UK

Abstract

In this work, a Rolling-Ball Viscometer/Densimeter is used to measure high-pressure, high-temperature (HPHT) density and viscosity data from 298.2 to 532.6 K and pressures up to 300.0 MPa for three different diesel fuels. The densities and viscosities have combined expanded uncertainties of 0.6% and 2.5%, respectively, with a coverage factor, $k = 2$. Two of the diesels, Highly Paraffinic (HPF) and Highly Aromatic (HAR), contain a larger paraffinic and aromatic content relative to the others, and are standard engine test fuels. The third is a Ultra-Low Sulfur Diesel (ULSD) that resembles an unfinished commercial diesel. Detailed compositional information is also reported for each diesel that provides a basis for interpreting the impact of composition on density and viscosity at high pressures. Both density and viscosity data are correlated to Tait-type equations with uncertainties of 0.6% and 4.0%, respectively. The Tait equations provide a facile means to compare observed differences in the density-pressure and viscosity-pressure profiles of the three different diesels. Density data are modeled with the Perturbed-Chain Statistical Associating Fluid Theory (PC-SAFT) equation of state (EoS) with pure component parameters calculated representing diesel as a single, pseudo-component only requiring average molecular weight (M_{ave}) and hydrogen to carbon ratio ($R_{H/C}$) as inputs. Viscosity data are modeled reasonably well using entropy scaling coupled with the PC-SAFT EoS and information on the diesel M_{ave} and $R_{H/C}$. The HPHT viscosity data are also modeled reasonably well with Free Volume Theory (FVT) with model parameters correlated to M_{ave} and $R_{H/C}$.

Keywords: Viscosity, Density, pseudo-component, Diesel

1. Introduction

On a global level diesel engines currently consume ~5 million tons of fuel/day, which represents one of the most significant processes¹ reflected in annual energy sales. In addition this global level of diesel fuel consumption is responsible for 25% of annual CO₂ emissions, 41% of annual NO_x emissions, and 11% of annual PM₁₀ emissions². Although alternative engines powered by gasoline, electricity, or fuel cells, are being proposed, diesel engines maintain the dominant position for heavy-duty applications. The Organization of the Petroleum Exporting Countries expects present-day diesel fuel sales to increase by 10% by 2040³. The increased consumption of diesel fuels requires new strategies to maximize engine efficiency and to minimize pollutant emissions. Current common rail injection systems are being operated to injection pressures as high as 300 MPa⁴ and temperatures as great as 363 K⁵. However, following injection, the temperature and pressure experienced by the fuel within the injector nozzle and combustion chamber are typically defined using computational tools since they cannot be experimentally measured. For example, Salemi et al.⁶ used computation methods to show that the fuel temperature could increase by as much as 100 K due to viscous heating effects within the diesel injector nozzle. Therefore, the fuel temperature entering the combustion chamber could be as high as 463 K where the fuel is exposed to air which may be as hot as 1000 K. Ultimately the actual temperature of the resultant fuel spray depends on the heat and mass transfer processes occurring within the combustion chamber. Numerical simulations commonly used to modify and improve the performance of diesel injection systems rely on the availability of a fundamental fuel fluid properties data base with information on viscosity and density. Accurate physical descriptions of the complex flow within the nozzle and the spray within the combustion chamber are dependent on an accurate data base of high-pressure, high temperature (HPHT) diesel fluid properties. Currently, there is a paucity of

thermodynamic and transport property data for real world diesel fuels at extreme HPHT conditions.

Currently, only a handful of literature studies report HPHT viscosities and densities for diesel⁷⁻¹⁰. Aquing et al.⁷ employ a vibrating wire viscometer to measure diesel viscosities to 473 K and pressures of 340 MPa. Schaschke et al.¹⁰ utilize a falling body viscometer to measure diesel densities and viscosities to pressures as high as 500 MPa. Bair⁸ also utilizes a falling body viscometer to measure both densities and viscosities of petroleum diesel and biodiesel and their mixtures to 350 MPa. Duncan et al.⁹, employ an oscillating piston viscometer to measure diesel and biodiesel viscosities at temperatures from 283 to 373 K and pressures to 130 MPa. In the present study a Rolling Ball Viscometer/Densimeter (RBVD) is used to measure viscosities and densities simultaneously for three different diesel fuels at temperatures from 298 to 530 K and pressures to 300 MPa.

Diesel fuels are multicomponent mixtures whose composition depend on the geographical country of origin and batch-to-batch processing variations⁷. Diesel fluid property predictions are challenging since diesel compositional information is not typically available. In addition, high pressure operating conditions are expected to exacerbate the differences in fluid properties for diesel fuels since high fluid densities amplify intermolecular interactions. Consider, for example, the differences in viscosities for several different diesels reported by two different research groups. Schaschke, et al. measured the viscosity of five different diesel fuels obtained from two British refineries, but they did not report any composition information for the diesels¹⁰. In contrast, Aquing et al.⁷ reported viscosities along with detailed composition information on the diesels they investigated. Differences in the viscosity as large as 50% are observed when comparing results from these two studies at a fixed temperature and low pressures, and these differences increase to

as high as 140% at 270 MPa. It remains a significant challenge explaining the underlying reasons for the large differences in HPHT viscosities observed by both research groups if composition information is not available for each diesel investigated.

Several approaches are available for modeling the density of complex mixtures (e.g., diesel, biodiesel, crude oils, bitumens, heavy oils) including the application of an EoS, such as simple cubics (e.g., van der Waals^{11, 12}, Peng-Robinson¹³⁻¹⁵, Soave-Redlich-Kwong^{14, 16, 17}) and contemporary, but more complex equations (Elliott-Suresh-Donohue¹⁸, Soft-SAFT¹⁹, PC-SAFT²⁰⁻²², SAFT-VR²³, SAFT- γ Mie²⁴). To reduce computational complexity, several research groups propose estimating diesel properties with model predictions of well-characterized, surrogate mixtures consisting of a minimum number of components. For example, Lin and Tavlarides²⁵ use the Benedict-Webb-Rubin^{25, 26} EoS with multiple pure-component parameters to predict HPHT densities for twenty diesel fuel surrogate mixtures containing one to fourteen compounds. In a different study Vidal et al.²⁷ uses the PC-SAFT EoS to predict the HPHT densities of four surrogate mixtures containing four to nine compounds where pure component PC-SAFT parameters are calculated using a group contribution (GC) method²⁸ or a correlation based on component molecular weight^{29, 30}. Rokni et al.²⁰ further reduce the number of compounds in the surrogate mixture by predicting HPHT diesel density using a single, pseudo-component technique based on the PC-SAFT EoS. This approach requires input of only two measured or calculated mixture properties: the number average molecular weight (M_{ave}) and the hydrogen to carbon ($R_{H/C}$) ratio, both of which are typically obtained from gas chromatography and elemental analyses. The approach reported by Rokni et al. is used to model the HPHT diesel densities measured in the present study.

There are also several methods for modeling the viscosity of complex mixtures, including expanded fluid theory³¹⁻³⁴, friction theory³⁵⁻³⁹, free volume theory (FVT)^{40,41}, hard sphere models⁴²⁻⁴⁴, residual entropy scaling^{45, 46}, Eyring's absolute rate theory^{47, 48}, and GC methods⁴⁹⁻⁵². However, only a few modeling approaches allow for diesel viscosity predictions based on composition. Aquing et al.⁷ modeled the viscosity of two diesel fuels using the GC methods of van Velzen et al.⁴⁹ and Sastri and Rao⁵⁰. Aquing's approach requires the input of multiple pure component parameters for each of the 140 compounds in the diesel fuels measured by 2-dimensional gas chromatography. Vidal et al.²⁷ predict the HPHT viscosities of four diesel surrogate mixtures using the GC residual entropy scaling method of Lötgering-Lin and Gross⁴⁶ that requires the input of pure component parameters for each compound in the mixture. Lin and Tavlarides²⁵ predict the viscosities of twenty surrogate mixtures using friction theory that involves fitting pure component parameters for each compound in the mixture. Rokni, et al.⁴⁵ predict the viscosities of two diesel fuels using a single, pseudo-component technique based on the GC residual entropy scaling approach of Lötgering-Lin and Gross⁴⁶. The approach of Rokni et al. requires up to three measured or calculated inputs for each diesel fuel: M_{ave} , $R_{H/C}$, and in one variation of the method, a single viscosity data point at a chosen reference state. The approach reported by Rokni et al. is used to model the HPHT diesel viscosities measured in the present study.

A RBVD apparatus is used here to simultaneously measure viscosities and densities at temperatures from 298.2 to 532.6 K and pressures up to 300.0 MPa for three different diesels. The resultant experimental uncertainty of the RBVD data is directly proportional to the availability of a calibration fluid with highly accurate viscosity/density data at HPHT conditions and with a viscosity profile similar to that expected for the fluid of interest. To circumvent the use of a

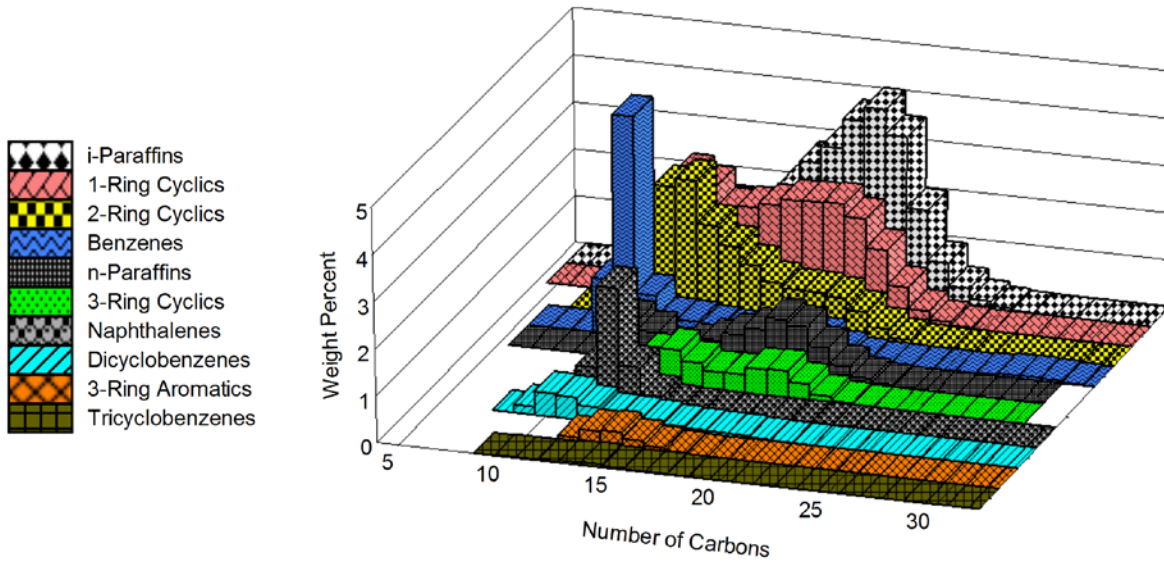
calibration fluid, a previously reported universal calibration method is used in the present study. This universal RBVD calibration method uses data for each diesel obtained directly with the RBVD and, in some instances, uses an independently measured diesel viscosity at 298.15 K and 0.1 MPa. This RBVD universal calibration approach results in reliable HPHT data and minimizes the impact of composition differences of the three diesels on the calibration relative to using a single calibration fluid⁵³. HPHT viscosity and companion density data are reported along with diesel compositional information that allows for an opportunity to relate diesel composition to the observed fluid properties. Composition information also allows for an evaluation of equation of state (EoS) and transport models used to predict HPHT densities and viscosities. As mentioned, the pseudo-component approaches reported by Rokni et al.^{20, 45} is used to model the HPHT diesel viscosities and densities obtained in this study. The resultant viscosity data are also modeled using the Free Volume Theory (FVT) with input densities predicted from the PC-SAFT EoS. In addition, a correlation is proposed demonstrating that the three FVT parameters can be correlated to the M_{ave} and $R_{H/C}$ of each diesel.

2. Materials and Methods

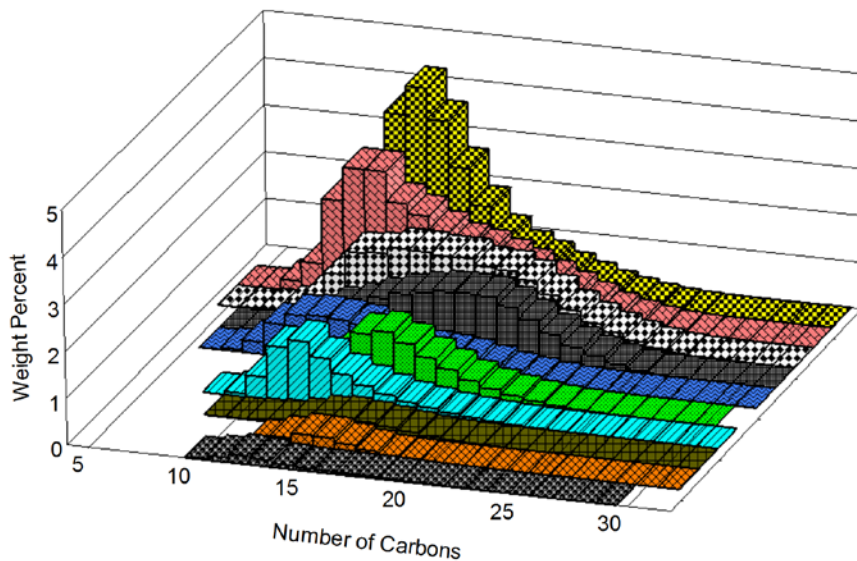
2.1. Materials

The three diesels used in this study are classified as Highly Paraffinic (HPF), Ultra-Low Sulfur Diesel (ULSD), and Highly Aromatic (HAR). Both HPF and HAR are standard engine test fuels. The designations HPF and HAR are meant to distinguish the relatively higher concentration of paraffins and aromatics only relative to the three diesels studied here. The Ultra-Low Sulfur Diesel (ULSD) is representative of a typical unfinished commercial diesel fuel.

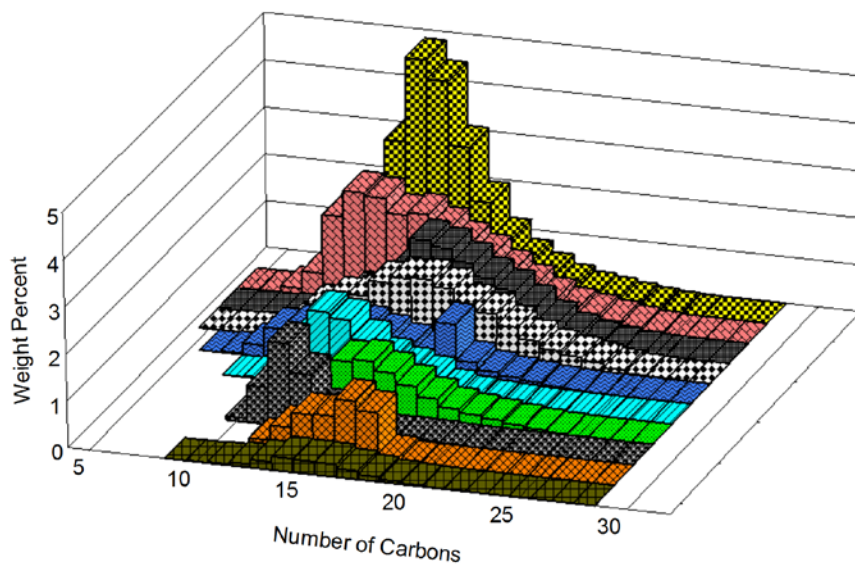
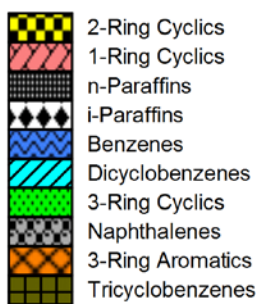
Triton Analytical Corporation performed gas chromatography on each diesel fuel, and this analysis provides information on the carbon number distribution, by weight percent, for several hydrocarbon chemical families prevalent in diesel fuel. The details of the gas chromatography procedure are described in detail elsewhere^{54, 55}. Figures 1(a) to 1(c) show the carbon number distribution by weight for the chemical families in HPF, ULSD, and HAR respectively. The Supplemental Information (SI) provides the chromatography data in tabular form. Note that in Figure 1 the grouping 3-ring aromatics includes acenaphthenes, anthracenes/phenanthrenes, phenanthrindene, and fluorenes/acenaphthylenes.



(a)



(b)



(c)

Figure 1. Carbon number distribution by weight for each chemical family present in the diesel fuels investigated in this study. (a) HPF, (b) ULSD, and (c) HAR.

Table 1 lists the hydrogen to carbon ratio, $R_{H/C}$, number average molecular weight, M_n , weight average molecular weight, M_w , average carbon number, CN_{ave} , and the carbon number dispersion, δ_{CN} , for the fuels used in the study. In this study M_{ave} is used generally to refer to both molecular weight averages M_n and M_w . The parameters $R_{H/C}$ and M_{ave} values are reported directly by Triton Analytical Corporation. Equations 1 and 2 are adapted from Aquino et al.⁷ to calculate CN_{ave} and δ_{CN} , respectively. Table 2 provides more details on the amount and compound class for each chemical family in the fuels.

$$CN_{ave} = \sum_i w_{CN,i} CN_i \quad (1)$$

$$\delta_{CN} = \sum_{i=1}^N w_{CN,i} |CN_i - CN_{ave}| \quad (2)$$

where $w_{CN,i}$ is the weight fraction of a molecule with a specific carbon number, CN_i .

Table 1. Hydrogen to carbon ratio, $R_{H/C}$, number average molecular weight, M_n , weight average molecular weight, M_w , average carbon number, CN_{ave} , and carbon number dispersion, δ_{CN} , for HPF, ULSD, and HAR diesels investigated in this study.

Diesel	$R_{H/C}$	$M_n/g \cdot mol^{-1}$	$M_w/g \cdot mol^{-1}$	CN_{ave}	δ_{CN}
HPF	1.91	199.2	212.0	15.2	3.10
ULSD	1.89	188.1	199.9	14.4	2.92
HAR	1.81	185.8	194.5	14.1	2.40

Table 2. Listed here for each fuel investigated in this study are the total weight percent, W_{CF} , the averaged carbon number, CN_{ave} , and carbon number dispersion, δ_{CN} , for each chemical family in the fuel.

Chemical Family	$W_{CF}/\%$			$CN_{ave} \pm \delta_{CN}$		
	HPF	ULSD	HAR	HPF	ULSD	HAR
<i>n</i> -Paraffins	8.00	13.11	13.01	16.4 ± 2.6	16.1 ± 2.9	15.2 ± 2.4
<i>i</i> -Paraffins	28.36	18.06	13.53	17.2 ± 2.5	15.5 ± 3.2	15.0 ± 3.0
1-ring Cyclics	23.89	21.77	18.72	15.4 ± 2.7	13.4 ± 3.1	13.2 ± 2.7
2-ring Cyclics	16.38	22.09	22.13	14.1 ± 2.5	13.6 ± 2.2	13.4 ± 1.9
3-Ring Cyclics	4.81	7.05	6.02	15.9 ± 2.4	15.9 ± 2.0	15.8 ± 2.7
Benzenes	10.59	7.88	8.18	12.4 ± 3.1	13.3 ± 2.9	13.6 ± 2.8
Tetralins/indanes	2.36	6.50	7.56	12.5 ± 2.3	13.3 ± 2.1	13.6 ± 1.8
Tricyclobenzenes	0.27	1.43	1.51	13.8 ± 1.8	15.5 ± 1.8	15.3 ± 1.6
Naphthalenes	4.24	0.86	4.65	12.4 ± 0.8	14.2 ± 2.5	12.6 ± 1.1
Acenaphthenes	0.97	1.04	4.10	14.2 ± 1.2	14.8 ± 1.3	15.4 ± 1.3
Fluorenes/ Acenaphthylenes	0.04	0.11	0.27	14.6 ± 1.3	15.5 ± 1.3	14.7 ± 1.2
Anthracenes/ Phenanthrenes	0.01	0.05	0.18	14.8 ± 0.8	15.2 ± 0.8	14.6 ± 0.7
Phenanthrindene	< 0.01	< 0.01	< 0.01	16.3 ± 0.5	16.5 ± 0.7	15.8 ± 0.4
Heteroatoms	0.08	0.05	0.13	12.2 ± 0.7	12.3 ± 2.6	11.7 ± 1.4

2.2 Rolling–Ball Viscometer/Densimeter (RBVD)

The main features of the RBVD, shown in Figure 2, are summarized here and described in detail elsewhere⁵⁶⁻⁵⁹. The RBVD, constructed from Inconel 718, has an inside diameter (ID) of 1.5875 cm and an internal volume fixed by the contraction/expansion of a metal bellows (1.72 cm OD, BellowsTech LLC). A high-pressure generator (Model 37-5.75-60, HIP Inc.) delivers/removes water from the bellows that fixes the bellows position and the system pressure, measured with two transducers (Model 245-BMSPW, accurate to ± 0.07 MPa, for pressures to 69 MPa and Model 245-BZS, accurate to ± 0.41 MPa, for pressures to 414 MPa, Viatran Corp.). The RBVD internal temperature is measured at locations T1 and T2 with type-K thermocouples calibrated against a standard (BetaProbe TI+, precision to 0.01 K, accuracy to 0.06 K, Martel Electronics Corp.). For 17 out of 18 sets of isothermal data at temperatures below 425 K, each location is ± 0.1 K, one isotherm is ± 0.2 K, and the temperature difference between each location is ± 0.1 K. For three sets of isothermal data at temperatures near 525 K, each location is ± 0.5 K or less and the temperature difference between each location is ± 0.3 K.

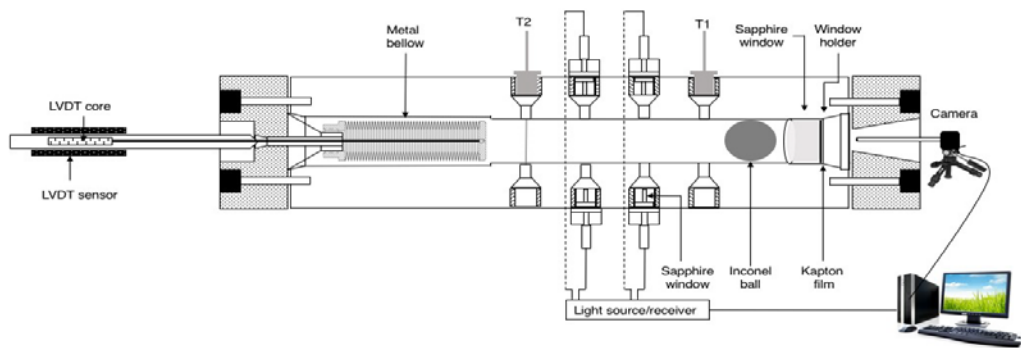


Figure 2. Schematic diagram of the windowed, rolling–ball viscometer/densimeter used in this study. T1 and T2 are thermocouples.

The bellows position is measured with a linear, variable, differential transformer (LVDT, Model 1000-HR, accurate to 0.102 mm, Measurement Specialties Inc.) attached to the end of the RBVD^{60,61}. An LVDT core piece, secured to one end of a solid rod, is pulled/pushed through the sensor region of the LVDT by the rod connected to the inner face of the bellows. The RBVD cell volume is correlated to the position of the bellows through a calibration procedure described in detail elsewhere⁵³. Therefore, the solution density is equal to the mass loaded into the cell divided by the volume of the cell at a given p - T condition. The combined expanded uncertainty of the density is $0.006 \cdot \rho$ ($\text{kg}\cdot\text{m}^{-3}$) with a coverage factor, $k = 2$.

The ball (Industrial Tectonics Inc.) used with the RBVD is also made of Inconel 718 and has an outside diameter (OD) of 1.5796 cm, which fixes the ball OD to RBVD ID (d/D) ratio at 0.995. A borescope is positioned against the sapphire window at the front of the RBVD and used to visually determine a single fluid phase exists and the ball rolls rather than slides during each measurement. A fiber optic, light transmittance-detection apparatus (sensor: Model R55FVWQ; cables: Model IF23SM900, Banner Engineering Corp.) is interfaced with a data acquisition program to measure the ball roll time (± 0.001 s) between two sets of opposing ports fitted with sapphire windows^{62,63}. A universal viscosity calibration approach described in detail elsewhere⁵³ is used here and the performance of this calibration approach is assessed in the proceeding section. The combined expanded uncertainty of the viscosity is $0.025 \cdot \eta$ ($\text{mPa}\cdot\text{s}$) with a coverage factor, $k = 2$.

Viscosities and densities are measured at 0.1 MPa using a Stabinger viscometer (Model SVM 3001, Anton Parr) according to ASTM D7042⁶⁴. The Stabinger viscometer is limited to fluids exhibiting densities within 600 to 3000 $\text{kg}\cdot\text{m}^{-3}$ and kinematic viscosities within 0.2 to 30,000

$\text{mm}^2 \cdot \text{s}^{-1}$. Temperature fluctuations on the Stabinger viscometer are maintained within 0.03 K from 288 to 373 K. Anton Parr USA Inc. specify that the Stabinger viscometer provides densities accurate to $0.1 \text{ kg} \cdot \text{m}^{-3}$ and viscosities accurate to $0.0035 \cdot \eta$ (mPa•s). However, in the present study triplicate density and viscosity measurements exhibited standard deviations of 0.13% and 0.48% of the measured property values, respectfully. Therefore, in accordance with guidelines specified in GUM⁶⁵ the expanded uncertainties are listed as $0.0026 \cdot \rho \text{ kg} \cdot \text{m}^{-3}$ and $0.01 \cdot \eta$ mPa•s, each with a coverage factor, $k = 2$.

2.3 Universal Calibration for the RBVD

Equation 3 shows the RBVD governing viscosity equation.

$$\eta = K \cdot t \cdot (\rho_b - \rho_{fl}) \sin\theta \quad (3)$$

where K is the calibration parameter defined by equation 4, t is ball roll time, ρ_b is the density of the Inconel ball, ρ_{fl} is the density of the fluid of interest, and θ is angle of inclination of the RBVD. As described in our previous study⁵³, the effect of the T and p on K is determined using the following relationship,

$$K = \left[1 + 2\beta(T-T_0) + C \left[\ln \left(\frac{p}{p_0} \right) \right] \left(\frac{D+p}{D+p_0} \right)^E \right] K_0 \quad (4)$$

where β is the coefficient of thermal expansion of Inconel 718⁶⁶, T_0 is a reference temperature fixed to 298 K, p_0 is a reference pressure fixed to 0.1 MPa, and C , D , and E are previously

determined, temperature-dependent parameters⁵³. Rowane and coworkers⁵¹ demonstrate that K_0 (298 K, 0.1 MPa) is dependent on the properties of the fluid of interest and can be calculated using the correlation shown in equation 5,

$$K_0 = e^{-[mx+b]} \quad (5)$$

where $x = [\rho_{fl}^{-3.36} \cdot \ln(t \cdot (\rho_b - \rho_{fl}) \cdot \sin\theta)]^{-1}$ (298 K, 0.1 MPa) and m and b are previously determined constants. Rowane showed this calibration method is valid for normal and branched paraffins ranging in molecular weight from octane to squalane. However, the correlation was not verified, as yet, for other types of compounds, such as aromatics and saturated cyclics, or for hydrocarbon mixtures. Alternatively, K_0 can be determined experimentally ($K_{0,exp}$) as briefly described here with details found elsewhere⁵³. Here we compare $K_{0,exp}$ and calculated values ($K_{0,calc}$) using the correlation (equation 5) with the previously reported constants.

Figure 3 shows that HPHT RBVD data at 298 K for all three diesels varies linearly with pressure, which is behavior observed previously for pure compounds. The curves in Figure 3 can be reliably extrapolated to determine $[\rho_{fl}^{-3.36} \cdot \ln[t \cdot (\rho_b - \rho_{fl}) \cdot \sin\theta]]_{p=0.1 \text{ MPa}}$ at 298 K, and $K_{0,calc}$ can now be calculated using the correlation shown as equation 5. Table 3 lists diesel densities and viscosities at 0.1 MPa from 298 to 343 K obtained in this study with the Stabinger viscometer. $K_{0,exp}$ can now be determined using equation 3 with Stabinger values for the viscosity and density and with RBVD values for $[\rho_{fl}^{-3.36} \cdot \ln[t \cdot (\rho_b - \rho_{fl}) \cdot \sin\theta]]_{p=0.1 \text{ MPa}}$, all at 298 K and 0.1 MPa. Table 4 lists $K_{0,exp}$ and $K_{0,calc}$ and the deviation between these two values. Interestingly, $K_{0,calc}$ and $K_{0,exp}$ values are in close agreement for the HPF and HAR. However, there is a significant deviation

between these values for the ULSD. It is important to recognize that the universal calibration equation was developed using only n-paraffins and iso-paraffins yet, as with all of the fuels, the GC characterization does not offer enough details to identify the non-paraffinic group that causes the deviation from our correlation. Further studies are in progress to test the correlation against well-characterized saturated cyclics and aromatics with and without linear and bulky alkyl side chains. Therefore, the HPHT ULSD viscosities presented here are determined using $K_{0,exp}$ since this parameter only depends on directly measured RBVD data and Stabinger viscosity and density data.

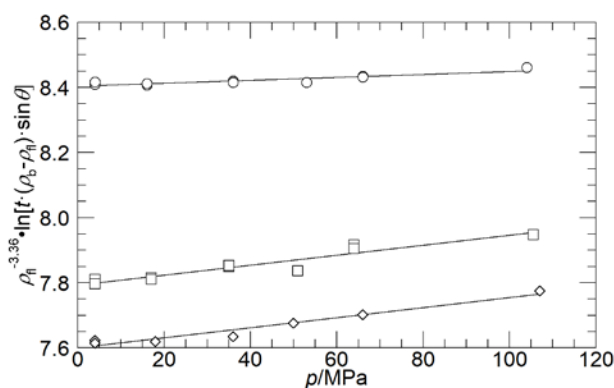


Figure 3. Linear pressure response of HPHT RBVD data recast as $[\rho_{fl}^{-3.36} \cdot \ln[t \cdot (\rho_b - \rho_{fl}) \cdot \sin \theta]]$ at 298 K obtained in this study for \circ - HPF, \square - ULSD, and \diamond - HAR. Lines are drawn to guide the eye.

Table 3. Densities and viscosities obtained in this study at 0.1 MPa from 298.15 to 343.15 K using a Stabinger viscometer.

HPF	ULSD	HAR
-----	------	-----

T/K	$\rho/ \text{kg}\cdot\text{m}^{-3}$	$\eta/ \text{mPa}\cdot\text{s}$	$\rho/ \text{kg}\cdot\text{m}^{-3}$	$\eta/ \text{mPa}\cdot\text{s}$	$\rho/ \text{kg}\cdot\text{m}^{-3}$	$\eta/ \text{mPa}\cdot\text{s}$
298.15	827.0	3.263	834.6	2.915	837.8	2.510
313.15	816.5	2.320	822.5	2.092	827.0	1.835
323.15	809.7	1.896	815.3	1.722	822.4	1.524
333.15	803.0	1.583	808.4	1.447	812.9	1.289
343.15	795.6	1.342	801.3	1.234	805.9	1.106

^a Standard uncertainties, u , for the Stabinger viscometer (Anton Parr SVM 3001) are $u(T) = 0.03 \text{ K}$, $U(\rho) = 0.0026 \cdot \rho \text{ kg}\cdot\text{m}^{-3}$, and $U_c(\eta) = 0.010 \cdot \eta \text{ mPa}\cdot\text{s}$ each with a coverage factor, $k = 2$.

Table 4. Comparison of experimentally determined $K_{0,\text{exp}}$ to calculated $K_{0,\text{calc}}$ values using the correlation given by equation 3 and parameters from a previous study.

Fuel	$K_{0,\text{exp}}$	$K_{0,\text{calc}}$	$100 \cdot (K_{0,\text{exp}} - K_{0,\text{calc}})/K_{0,\text{exp}} (\%)$
HPF	3.8512	3.9302	-2.1
ULSD	4.2080	3.8678	8.2
HAR	3.8131	3.8383	-1.2

3. Experimental Results

3.1 Densities and Viscosities

Tables 5 to 7 report densities and viscosities obtained in this study from 298.2 to 532.6 K and to pressures of 300 MPa for HPF, ULSD, and HAR. Although the densities and viscosities are listed in an increasing order of pressure, the data are obtained in a non-monotonic manner to minimize potential experimental artifacts. Figures 4(a) to 4(f) show the effect of pressure on the

densities (a to c) and viscosities (d to f) for HPF, ULSD, and HAR which show the range of conditions for which viscosity and density data are reported for each diesel.

In the following sections the density and viscosity data for each diesel are fit to correlations used to interpolate data sets at nominal temperatures to highlight interesting density-pressure and viscosity-pressure trends. In addition single, pseudo-component models, which consider only M_{ave} and $R_{H/C}$, are tested to determine if they can accurately depict density-pressure and viscosity-pressure trends.

Table 5. Highly Paraffinic (HPF) diesel densities and viscosities obtained in this study at temperatures ranging from 298.3 to 528.7 K and pressures up to 300.0 MPa.

p/MPa	$\rho/(\text{kg}\cdot\text{m}^{-3})$	$\eta/(\text{mPa}\cdot\text{s})$	p/MPa	$\rho/(\text{kg}\cdot\text{m}^{-3})$	$\eta/(\text{mPa}\cdot\text{s})$
		298.3	± 0.1 K		
3.8	827	3.417	140.1	895	19.605
3.9	827	3.432	140.7	896	19.985
16.4	835	4.124	171.3	907	28.598
16.5	835	4.114	175.5	909	29.173
35.6	847	5.427	176.1	909	29.42
35.7	847	5.416	211.9	921	44.315
52.9	856	6.797	231.1	927	54.405
65.6	863	8.068	254.1	934	69.293
65.7	863	8.091	273.3	940	83.044
104.0	881	12.980	274.2	940	85.877
106.3	882	13.075	299.9	947	111.973
106.5	882	13.289			
		299.6	± 0.1 K		
4.2	827	3.230	56.4	858	6.738
4.3	827	3.281	56.4	857	6.658
15.2	834	3.838	84.3	871	9.530
15.2	834	3.857	84.3	871	9.603
27.8	842	4.627	109.8	882	13.073
27.9	842	4.619	135.3	892	17.784
55.7	857	6.764			

^a Standard uncertainties u are $u(p) = 0.07$ MPa at $p \leq 68.9$ MPa and 0.41 MPa at $p > 68.9$ MPa. The combined expanded uncertainties U_c are $U_c(\rho) = 0.006 \cdot \rho$ kg \cdot m⁻³, and $U_c(\eta) = 0.025 \cdot \eta$ mPa \cdot s each with a coverage factor, $k = 2$.

Table 5. Continued -- Highly Paraffinic (HPF) diesel densities and viscosities.

p/MPa	$\rho/(\text{kg}\cdot\text{m}^{-3})$	$\eta/(\text{mPa}\cdot\text{s})$	p/MPa	$\rho/(\text{kg}\cdot\text{m}^{-3})$	$\eta/(\text{mPa}\cdot\text{s})$
		323.2	± 0.1 K		
3.7	810	1.881	116.1	873	6.677
3.8	810	1.891	116.2	873	6.718
11.1	816	2.069	132.2	880	7.886
11.2	816	2.087	132.5	880	7.929
20.7	823	2.345	139.8	883	8.604
20.7	823	2.374	140.2	884	8.895
33.0	831	2.723	160.1	891	10.286
47.6	840	3.213	160.3	891	10.276
47.8	840	3.236	174.4	897	11.813
64.0	849	3.863	174.5	897	12.338
65.6	849	4.129	200.4	906	15.482
77.3	856	4.443	212.4	910	16.969
77.4	856	4.495	218.5	912	18.150
97.1	865	5.510	232.1	917	20.139
97.2	865	5.529	252.5	923	24.317
105.4	869	6.281	274.5	930	29.385
105.8	869	6.072	300.0	937	36.623
		350.4	± 0.1 K		
3.6	790	1.226	66.1	834	2.428
3.8	792	1.203	66.3	834	2.427
3.8	790	1.233	66.4	835	2.453
3.8	792	1.216	84.1	845	2.829

^a Standard uncertainties u are $u(p) = 0.07$ MPa at $p \leq 68.9$ MPa and 0.41 MPa at $p > 68.9$ MPa. The combined expanded uncertainties U_c are $U_c(\rho) = 0.006 \cdot \rho$ $\text{kg}\cdot\text{m}^{-3}$, and $U_c(\eta) = 0.025 \cdot \eta$ $\text{mPa}\cdot\text{s}$ each with a coverage factor, $k = 2$.

Table 5. Continued -- Highly Paraffinic (HPF) diesel densities and viscosities.

p/MPa	$\rho/(\text{kg}\cdot\text{m}^{-3})$	$\eta/(\text{mPa}\cdot\text{s})$	p/MPa	$\rho/(\text{kg}\cdot\text{m}^{-3})$	$\eta/(\text{mPa}\cdot\text{s})$
		350.4	± 0.1 K		
3.8	793	1.189	90.9	847	3.057
3.9	793	1.193	91.1	847	3.093
4.2	793	1.189	105.6	855	3.526
4.3	793	1.202	122.0	862	4.101
10.4	799	1.286	122.1	862	4.084
12.1	798	1.351	141.1	871	4.761
12.2	798	1.360	147.5	874	4.973
15.4	803	1.367	147.6	874	5.002
15.4	803	1.379	164.4	879	5.818
21.6	807	1.478	164.5	879	5.882
21.8	807	1.502	166.8	883	5.888
26.7	809	1.604	174.4	885	6.304
26.9	809	1.610	189.2	891	6.968
42.3	822	1.868	210.5	898	8.425
42.4	822	1.861	231.5	905	9.875
43.8	822	1.895	252.3	912	11.513
43.8	822	1.905	252.9	912	11.554
44.7	821	1.961	274.4	919	13.699
44.8	821	1.956	299.4	926	16.369

^a Standard uncertainties u are $u(p) = 0.07$ MPa at $p \leq 68.9$ MPa and 0.41 MPa at $p > 68.9$ MPa. The combined expanded uncertainties U_c are $U_c(\rho) = 0.006 \cdot \rho$ kg \cdot m⁻³, and $U_c(\eta) = 0.025 \cdot \eta$ mPa \cdot s each with a coverage factor, $k = 2$.

Table 5. Continued -- Highly Paraffinic (HPF) diesel densities and viscosities.

p/MPa	$\rho/(\text{kg}\cdot\text{m}^{-3})$	$\eta/(\text{mPa}\cdot\text{s})$	p/MPa	$\rho/(\text{kg}\cdot\text{m}^{-3})$	$\eta/(\text{mPa}\cdot\text{s})$
		433.1	± 0.1 K		
4.4	737	0.480	105.3	816	1.226
4.5	737	0.493	105.4	816	1.232
10.2	744	0.515	105.5	817	1.260
10.3	744	0.528	105.8	817	1.257
22.1	757	0.588	124.8	827	1.463
22.3	757	0.601	125.2	827	1.463
30.1	766	0.655	126.5	828	1.433
30.2	766	0.662	140.9	835	1.578
35.8	770	0.685	141.0	835	1.572
35.9	770	0.688	147.0	838	1.692
44.2	777	0.731	147.1	838	1.693
44.2	777	0.747	175.2	850	2.036
64.2	790	0.901	175.5	850	2.047
64.2	790	0.894	175.7	851	1.990
64.4	790	0.904	175.9	851	1.989
64.4	790	0.910	194.4	858	2.284
64.8	793	0.879	210.9	865	2.482
65.0	793	0.890	211.1	865	2.473
65.7	792	0.894	241.7	877	2.968
65.8	792	0.899	242.2	877	2.976
85.8	805	1.084			

^a Standard uncertainties u are $u(p) = 0.07$ MPa at $p \leq 68.9$ MPa and 0.41 MPa at $p > 68.9$ MPa. The combined expanded uncertainties U_c are $U_c(\rho) = 0.006 \cdot \rho$ $\text{kg}\cdot\text{m}^{-3}$, and $U_c(\eta) = 0.025 \cdot \eta$ $\text{mPa}\cdot\text{s}$ each with a coverage factor, $k = 2$.

Table 5. Continued -- Highly Paraffinic (HPF) diesel densities and viscosities.

p/MPa	$\rho/(\text{kg}\cdot\text{m}^{-3})$	$\eta/(\text{mPa}\cdot\text{s})$	p/MPa	$\rho/(\text{kg}\cdot\text{m}^{-3})$	$\eta/(\text{mPa}\cdot\text{s})$
		528.7	± 0.3 K		
3.8	662	0.228	74.4	755	0.513
3.9	662	0.226	74.7	755	0.516
3.9	662	0.236	97.8	770	0.598
4.0	662	0.237	98.1	770	0.608
8.9	673	0.249	100.3	772	0.608
9.1	673	0.258	101.2	772	0.595
21.2	693	0.294	131.2	790	0.758
21.4	694	0.305	131.5	790	0.759
21.6	698	0.304	140.8	796	0.785
21.7	698	0.308	141.0	796	0.791
34.3	711	0.350	166.5	810	0.938
35.5	715	0.347	167.4	810	0.947
35.7	715	0.347	175.5	814	0.964
35.9	715	0.358	175.7	814	0.971
36.0	715	0.359	190.8	822	1.089
51.5	732	0.412	191.2	822	1.075
52.5	733	0.407	199.3	825	1.101
53.1	733	0.420	199.5	826	1.105
57.4	734	0.422	223.6	836	1.252
57.7	735	0.434	223.8	836	1.260
64.7	744	0.451	244.3	845	1.395
65.0	745	0.464			

^a Standard uncertainties u are $u(p) = 0.07$ MPa at $p \leq 68.9$ MPa and 0.41 MPa at $p > 68.9$ MPa. The combined expanded uncertainties U_c are $U_c(\rho) = 0.006 \cdot \rho$ kg \cdot m⁻³, and $U_c(\eta) = 0.025 \cdot \eta$ mPa \cdot s each with a coverage factor, $k = 2$.

Table 6. Ultra-Low Sulfur Diesel (ULSD) densities and viscosities obtained in this study at temperatures ranging from 298.2 to 525.4 K and pressures up to 275.4 MPa.

p/MPa	$\rho/(\text{kg}\cdot\text{m}^{-3})$	$\eta/(\text{mPa}\cdot\text{s})$	p/MPa	$\rho/(\text{kg}\cdot\text{m}^{-3})$	$\eta/(\text{mPa}\cdot\text{s})$
298.2			$\pm 0.1 \text{ K}$		
3.8	836	3.085	64.4	869	6.993
3.8	836	3.062	64.5	869	7.049
16.8	844	3.697	105.5	886	11.134
16.8	844	3.688	140.9	899	16.645
35.3	854	4.809	174.8	910	24.746
35.3	854	4.796	200.0	918	32.373
51.0	862	5.750	221.0	924	40.310
51.0	862	5.742	244.9	930	52.202
299.7			$\pm 0.1 \text{ K}$		
4.0	835	2.914	84.8	877	8.318
21.5	843	3.667	107.7	887	11.068
21.7	843	3.660	132.3	897	15.005
49.6	860	5.308	156.0	906	19.149
323.2			$\pm 0.1 \text{ K}$		
3.8	821	1.750	141.7	887	7.820
17.3	829	2.080	175.0	899	10.620
35.1	839	2.570	199.4	907	13.230
48.8	847	2.980	223.5	914	16.400
65.8	856	3.600	245.3	920	19.980
106.2	874	5.450	259.4	924	22.420
141.7	887	7.770	274.7	928	25.610

^a Standard uncertainties u are $u(p) = 0.07 \text{ MPa}$ at $p \leq 68.9 \text{ MPa}$ and 0.41 MPa at $p > 68.9 \text{ MPa}$. The combined expanded uncertainties U_c are $U_c(\rho) = 0.006 \cdot \rho \text{ kg}\cdot\text{m}^{-3}$, and $U_c(\eta) = 0.025 \cdot \eta \text{ mPa}\cdot\text{s}$ each with a coverage factor, $k = 2$.

Table 6. Continued -- ULSD diesel densities and viscosities.

p/MPa	$\rho/(\text{kg}\cdot\text{m}^{-3})$	$\eta/(\text{mPa}\cdot\text{s})$	p/MPa	$\rho/(\text{kg}\cdot\text{m}^{-3})$	$\eta/(\text{mPa}\cdot\text{s})$
		325.5	± 0.1 K		
3.6	817	1.706	49.6	845	2.945
22.3	829	2.196	83.8	863	4.332
49.3	845	3.005	106.2	874	5.385
49.3	845	2.965	133.1	886	7.130
		348.3	± 0.1 K		
3.6	804	1.180	141.7	876	4.492
3.7	804	1.179	162.5	888	5.558
24.7	819	1.527	162.9	888	5.595
35.4	824	1.693	175.1	883	5.916
49.1	833	1.981	199.3	896	7.121
49.3	833	1.967	224.8	900	8.747
65.1	841	2.269	245.2	910	10.077
84.1	853	2.792	246.0	907	10.295
104.5	860	3.264	263.0	911	11.599
105.6	864	3.358	275.4	919	12.649
133.6	876	4.376			

^aStandard uncertainties u are $u(p) = 0.07$ MPa at $p \leq 68.9$ MPa and 0.41 MPa at $p > 68.9$ MPa. The combined expanded uncertainties U_c are $U_c(\rho) = 0.006 \cdot \rho$ kg \cdot m⁻³, and $U_c(\eta) = 0.025 \cdot \eta$ mPa \cdot s each with a coverage factor, $k = 2$.

Table 6. Continued -- ULSD diesel densities and viscosities.

p/MPa	$\rho/(\text{kg}\cdot\text{m}^{-3})$	$\eta/(\text{mPa}\cdot\text{s})$	p/MPa	$\rho/(\text{kg}\cdot\text{m}^{-3})$	$\eta/(\text{mPa}\cdot\text{s})$
		434.9	± 0.1 K		
3.9	741	0.470	116.9	829	1.286
3.9	741	0.470	117.0	827	1.259
4.4	746	0.473	117.2	827	1.256
22.6	762	0.582	135.3	836	1.421
34.3	776	0.656	141.4	843	1.524
49.4	786	0.752	157.2	847	1.654
77.7	812	0.945	175.4	858	1.885
86.1	812	0.979	175.6	858	1.911
86.2	812	0.986	199.9	868	2.208
86.2	812	1.023	224.3	877	2.527
86.4	812	1.023	245.0	885	2.844
106.7	827	1.193			
		525.4	± 0.5 K		
3.6	680	0.255	106.0	782	0.644
3.8	681	0.262	141.6	804	0.817
17.3	708	0.308	141.6	804	0.809
35.3	732	0.369	141.8	803	0.808
35.3	732	0.371	176.6	820	1.005
49.0	747	0.417	176.6	820	0.995
49.4	740	0.418	198.5	829	1.121
64.1	751	0.473	217.2	837	1.255
105.8	783	0.649	217.3	837	1.244

^a Standard uncertainties u are $u(p) = 0.07$ MPa at $p \leq 68.9$ MPa and 0.41 MPa at $p > 68.9$ MPa. The combined expanded uncertainties U_c are $U_c(\rho) = 0.006 \cdot \rho$ $\text{kg}\cdot\text{m}^{-3}$, and $U_c(\eta) = 0.025 \cdot \eta$ $\text{mPa}\cdot\text{s}$ each with a coverage factor, $k = 2$.

Table 7. Highly Aromatic (HAR) densities and viscosities obtained in this study at temperatures ranging from 298.4 to 532.6 K and pressures up to 262.2 MPa.

p/MPa	$\rho/(\text{kg}\cdot\text{m}^{-3})$	$\eta/(\text{mPa}\cdot\text{s})$	p/MPa	$\rho/(\text{kg}\cdot\text{m}^{-3})$	$\eta/(\text{mPa}\cdot\text{s})$
		298.4	± 0.1 K		
4.0	842	2.689	66.6	875	6.371
4.0	842	2.732	106.6	892	10.054
17.8	852	3.290	142.2	905	15.610
18.5	851	3.298	176.8	916	23.711
36.4	861	4.212	198.5	922	29.977
50.1	868	5.106	219.1	928	38.704
50.4	868	5.071	224.2	932	40.161
66.5	875	6.217			
		299.6	± 0.1 K		
4.2	840	2.640	50.2	865	4.908
4.2	840	2.628	101.0	889	9.241
16.5	847	3.141	146.6	907	15.591
29.7	854	3.739	174.2	917	21.543
50.0	865	4.867	199.3	926	28.827
		323.3	± 0.1 K		
4.0	828	1.609	102.9	878	4.843
4.4	826	1.614	106.5	882	5.041
4.8	827	1.614	138.9	894	6.975
16.7	834	1.883	141.5	896	7.092
16.8	834	1.887	171.4	906	9.563
17.3	836	1.896	175.9	908	9.983
35.0	848	2.322	196.0	915	12.054

^a Standard uncertainties u are $u(p) = 0.07$ MPa at $p \leq 68.9$ MPa and 0.41 MPa at $p > 68.9$ MPa. The combined expanded uncertainties U_c are $U_c(\rho) = 0.006 \cdot \rho$ $\text{kg}\cdot\text{m}^{-3}$, and $U_c(\eta) = 0.025 \cdot \eta$ $\text{mPa}\cdot\text{s}$ each with a coverage factor, $k = 2$.

Table 7. Continued -- Highly Aromatic (HAR) densities and viscosities

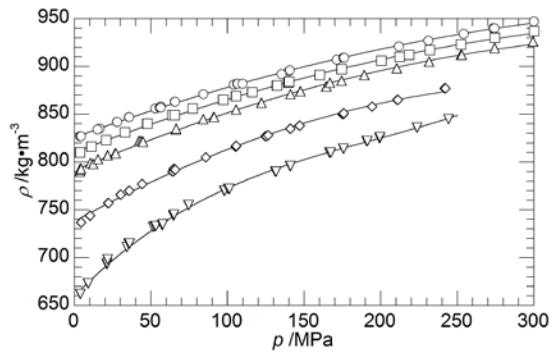
p/MPa	$\rho/(\text{kg}\cdot\text{m}^{-3})$	$\eta/(\text{mPa}\cdot\text{s})$	p/MPa	$\rho/(\text{kg}\cdot\text{m}^{-3})$	$\eta/(\text{mPa}\cdot\text{s})$
		323.3	± 0.1 K		
35.0	848	2.341	209.3	918	13.634
50.3	852	2.759	210.0	919	13.506
52.1	857	2.805	228.0	924	16.013
66.3	864	3.297	245.8	929	18.973
66.3	864	3.326	262.2	934	21.882
74.7	865	3.613			
		349.9	± 0.1 K		
4.2	814	1.046	140.8	882	3.999
16.6	822	1.216	175.2	895	5.253
35.9	833	1.492	211.0	907	7.108
51.1	841	1.754	227.0	912	7.951
65.4	847	2.005	245.6	917	9.287
65.4	847	2.024	258.8	921	10.139
105.3	867	2.913			
		350.5	± 0.2 K		
4.4	811	1.048	74.6	853	2.194
4.4	811	1.048	102.6	867	2.825
27.9	827	1.363	141.3	884	3.976
27.9	827	1.368	171.2	896	5.070
41.0	834	1.569	196.2	906	6.220
49.6	839	1.708			

^a Standard uncertainties u are $u(p) = 0.07$ MPa at $p \leq 68.9$ MPa and 0.41 MPa at $p > 68.9$ MPa. The combined expanded uncertainties U_c are $U_c(\rho) = 0.006 \cdot \rho$ $\text{kg}\cdot\text{m}^{-3}$, and $U_c(\eta) = 0.025 \cdot \eta$ $\text{mPa}\cdot\text{s}$ each with a coverage factor, $k = 2$.

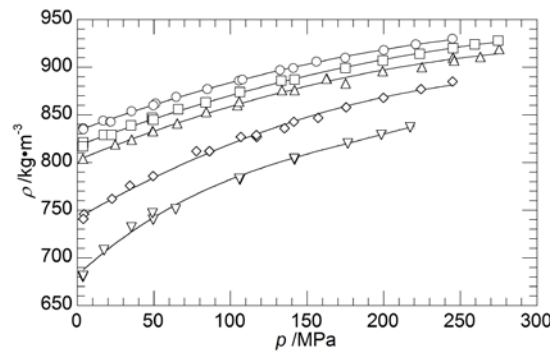
Table 7. Continued -- Highly Aromatic (HAR) densities and viscosities

p/MPa	$\rho/(\text{kg}\cdot\text{m}^{-3})$	$\eta/(\text{mPa}\cdot\text{s})$	p/MPa	$\rho/(\text{kg}\cdot\text{m}^{-3})$	$\eta/(\text{mPa}\cdot\text{s})$
		433.2	± 0.2 K		
3.8	754	0.434	101.6	831	1.069
4.0	754	0.440	101.8	831	1.070
28.4	779	0.569	146.2	853	1.442
28.6	779	0.574	170.4	865	1.691
50.2	798	0.697	196.7	876	2.003
75.0	816	0.856	196.7	876	2.015
75.3	816	0.864			
		532.6	± 0.4 K		
4.3	681	0.229	100.6	786	0.529
4.3	680	0.224	101.4	786	0.537
30.8	724	0.306	141.4	811	0.702
50.6	748	0.368	171.6	828	0.827
73.5	767	0.433	196.3	839	0.954

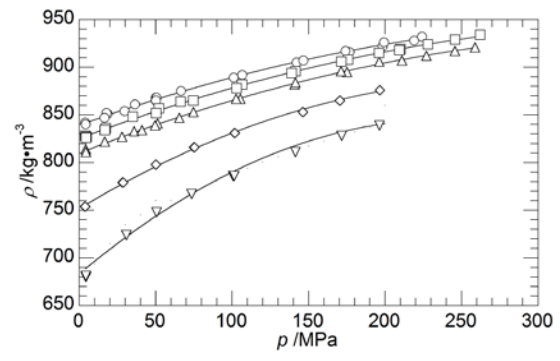
^a Standard uncertainties u are $u(p) = 0.07$ MPa at $p \leq 68.9$ MPa and 0.41 MPa at $p > 68.9$ MPa. The combined expanded uncertainties U_c are $U_c(\rho) = 0.006 \cdot \rho$ kg \cdot m $^{-3}$, and $U_c(\eta) = 0.025 \cdot \eta$ mPa \cdot s each with a coverage factor, $k = 2$.



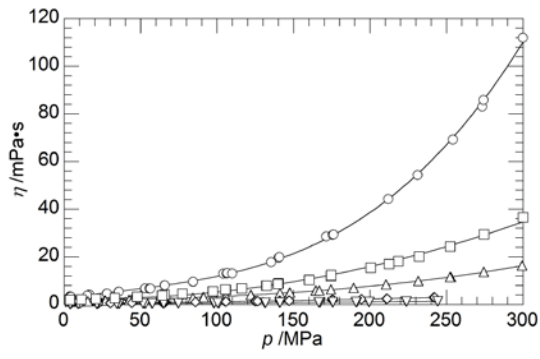
(a)



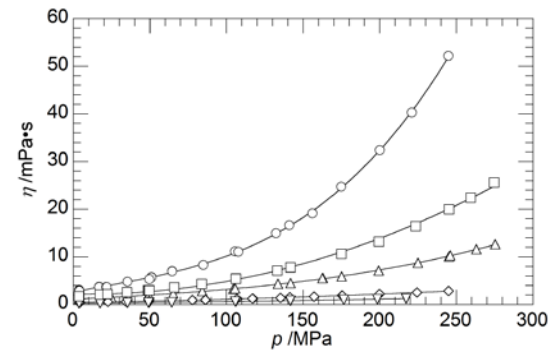
(b)



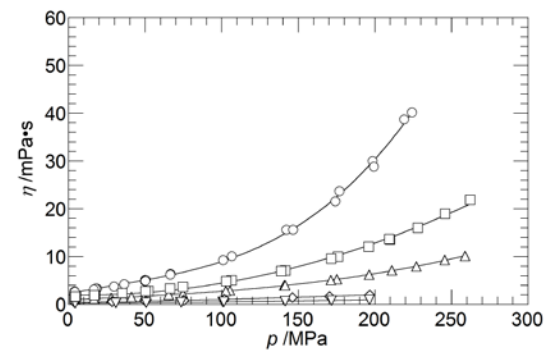
(c)



(d)



(e)



(f)

Figure 4. Effect of pressure on density (a) HPF, (b) ULSD, and (c) HAR and viscosity (d) HPF, (e) ULSD, and (f) HAR at approximately \circ - 298, \square - 323, \triangle - 350, \diamond - 433, and ∇ - 530 K obtained in the study (see Tables 5, 6, and 7 for exact temperatures). Lines are drawn to guide the eye.

3.2 Data Correlations

3.2.1 Tait Density Correlation

Density data obtained in this study are fit to the Tait equation shown in equation 6

$$\frac{\rho - \rho_0(T)}{\rho} = C \log_{10} \left(\frac{P + B(T)}{P_0 + B(T)} \right) \quad (6)$$

where C is a constant, ρ_0 is a temperature dependent density at $p_0 = 0.1$ MPa calculated by equation 7, and $B(T)$ is a temperature dependent parameter given by equation 8.

$$\rho_0(T)/kg \cdot m^{-3} = \sum_{i=0}^2 a_i T^i \quad (7)$$

$$B(T)/MPa = \sum_{i=0}^2 b_i T^i \quad (8)$$

Table 8 lists values for the parameters in equations 6 to 8 for each diesel. The procedure used to fit density data, described in detail elsewhere^{53, 59, 67}, involves minimizing the average absolute percent deviation (Δ_{AAD} , equation 9) and constraining the bias (Δ_{bias} , equation 10) to zero. The fit of the data is also characterized with values for the standard deviation (Δ_{SD} , equation 11) and the maximum deviation (Δ_{max} , equation 12).

$$\Delta_{AAD}/\% = 100 \cdot \frac{1}{N} \sum_{i=1}^N \left| \left(\frac{x_{i,exp} - x_{i,cal}}{x_{i,exp}} \right) \right| \quad (9)$$

$$\Delta_{bias}/\% = \frac{1}{N} \sum_{i=1}^N 100 \cdot \left(\frac{x_{i,exp} - x_{i,cal}}{x_{i,exp}} \right) \quad (10)$$

$$\Delta_{SD}/\% = \sqrt{\frac{\sum_{i=1}^n (\Delta_i - \Delta_{AAD})^2}{n-1}} \quad (11)$$

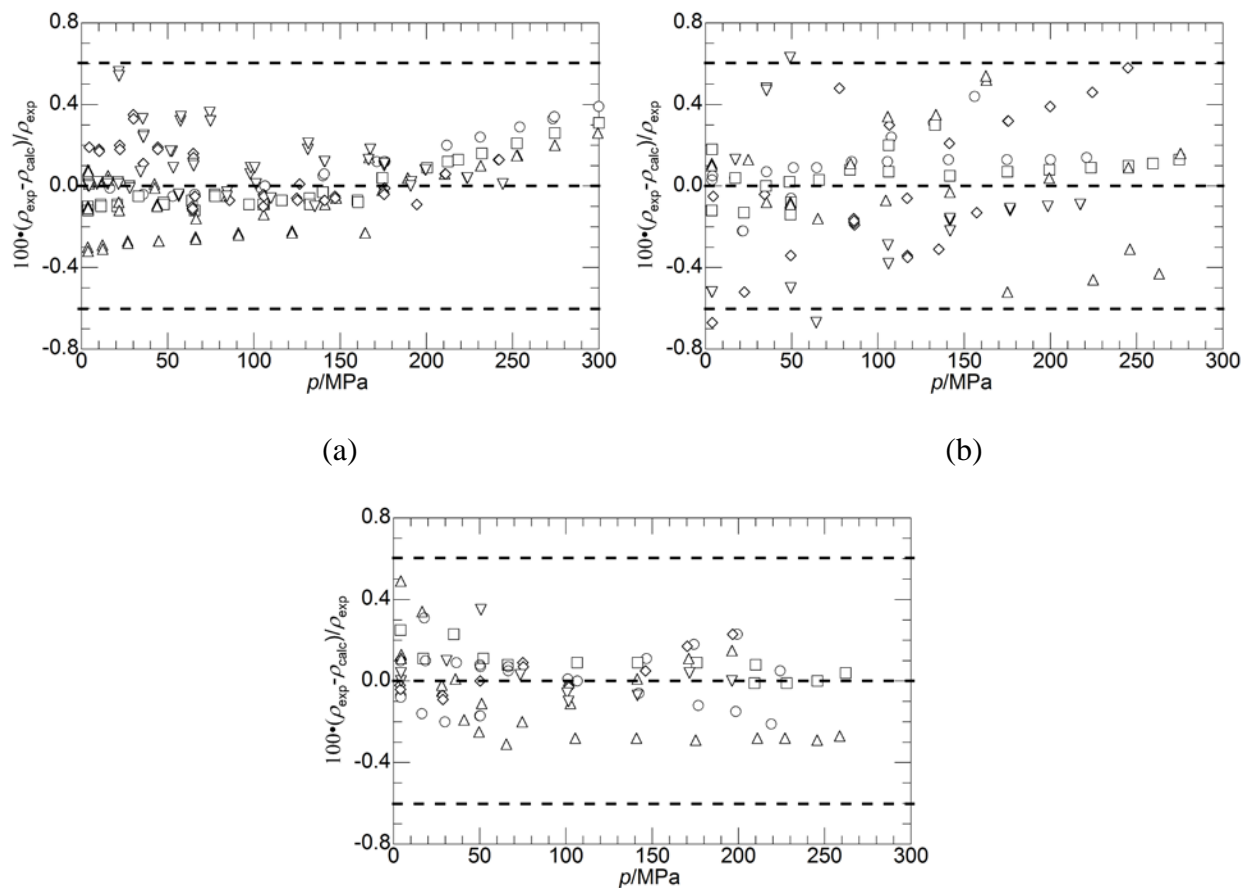
$$\Delta_{max}/\% = Max \left(100 \cdot \left(\left| \frac{x_{i,exp} - x_{i,cal}}{x_{i,exp}} \right| \right) \right) \quad (12)$$

where $x_{i,exp}$ and $x_{i,cal}$ are experimental and calculated data points, N is the total number of data points, and $\Delta_i = |x_{i,exp} - x_{i,cal}|$.

Table 8. Parameters for the modified Tait equation used to reproduce the densities of the three diesels considered in this study. The pressure and temperature ranges, parameters used with the Tait density equation, Δ_{AAD} , Δ_{SD} , Δ_{max} , and Δ_{bias} are listed for HPF, ULSD, and HAR diesels.

	HPF	ULSD	HAR
T_{range} / K	298.3 - 528.7	298.2 - 525.0	298.2 - 533.0
p_{range} / MPa	3.6 - 300.0	3.6 - 275.4	3.8 - 262.2
C	0.2202	0.2081	0.2163
$10^{-2} \cdot a_0 / kg \cdot m^{-3}$	9.7749	10.172	9.6319
$10^1 \cdot a_1 / kg \cdot m^{-3} \cdot K^{-1}$	-0.3834	-5.7986	-2.5290
$10^4 \cdot a_2 / kg \cdot m^{-3} \cdot K^{-2}$	-4.3527	-1.2725	-5.5598
$10^{-2} \cdot b_0 / MPa$	3.2524	3.7662	3.5593
$10^1 \cdot b_1 / (MPa/K)$	-9.2733	-11.165	-10.236
$10^4 \cdot b_2 / (MPa/K^2)$	6.7987	9.6105	7.5998
$\Delta_{AAD}/\%$	0.1	0.2	0.1
$\Delta_{SD}/\%$	0.1	0.2	0.1
$\Delta_{max}/\%$	0.6	0.7	0.5
$\Delta_{bias}/\%$	0.0	0.0	0.0

Figure 5 shows deviation plots comparing experimental densities for each diesel to densities calculated using the Tait equation with the parameters listed in Table 8. Dashed lines drawn at $\pm 0.6\%$ represent the combined expanded uncertainty of the density data determined in this study. Except for two ULSD density data points, the experimental and calculated densities for all three diesels obtained in this study agree within the experimental uncertainty of 0.6%. More than 95% of the density data obtained in this study compare within $\pm 0.6\%$, therefore values calculated with the Tait equation are given an uncertainty of $U_c(\rho) = 0.006 \cdot \rho$ with a coverage factor, $k = 2$. Note also that the value for the constant C found for the three diesels is reasonably close to values found by other research groups for several other hydrocarbon systems^{61, 67-69}.



(c)

Figure 5. Experimental density data (ρ_{exp}) compared to Tait-calculated densities (ρ_{calc}) for (a) HPF, (b) ULSD, and (c) HAR diesels at approximately \circ - 298, \square - 323, \triangle - 350, \diamond - 433, and ∇ - 530 K (see Tables 5, 6, and 7 for exact temperatures). The dashed lines at $\pm 0.6\%$ reflect the combined expanded experimental uncertainty for the densities where, $U_c(\rho) = 0.006 \cdot \rho$, with a coverage factor, $k = 2$.

Figure 6 shows the impact of pressure on density for the three diesels studied here at 298.2 K with a companion deviation plot showing the effect of pressure on the density difference between each grouping of two diesels. Figure 6 shows that at all pressures the HAR fuel exhibits the greatest density whereas the HPF fuel exhibits the lowest density, on average, which are trends that scale with decreasing M_{ave} and $R_{\text{H/C}}$. At the highest pressures the densities of the ULSD and HPF diesels are indistinguishable within our experimental uncertainty. The deviation graphs also show that the HPF density increases more rapidly with pressure than the HAR density although this difference eventually decreases to $\sim 1\%$ at the highest pressures. These density data suggest that ULSD is the most compressible and HPF the least compressible of the three fuels. Complementary graphs found in the SI show similar trends for diesel density data at 323.2, 353.2, 433.0, and 530.0 K.

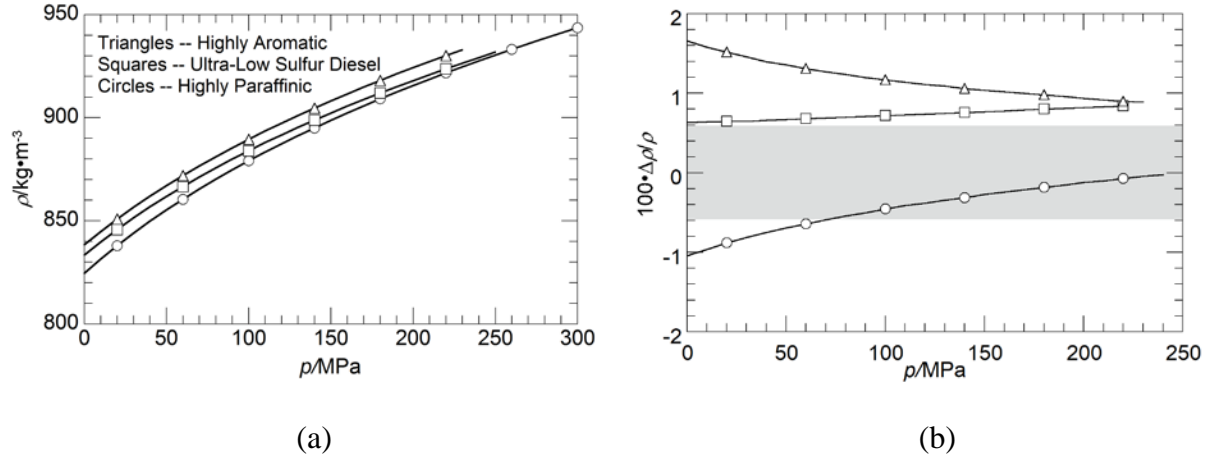


Figure 6. Comparison of Tait-calculated densities for three diesels at 298.2 K. (a) Impact of pressure on density with symbols on each line identifying a particular diesel where Δ - HAR, \square - ULSD, and \circ - HPF. (b) Deviation graph showing the effect of pressure on the difference ($100 \cdot \Delta\rho/\rho$) between sets of diesel densities with symbols on each line identifying a particular set of two diesels where \circ - $100 \cdot (\rho_{\text{HPF}} - \rho_{\text{ULSD}})/\rho_{\text{HPF}}$, \square - $100 \cdot (\rho_{\text{HAR}} - \rho_{\text{ULSD}})/\rho_{\text{HAR}}$, and Δ - $100 \cdot (\rho_{\text{HAR}} - \rho_{\text{HPF}})/\rho_{\text{HAR}}$. The gray box shows where the deviations fall within the combined expanded uncertainty of the Tait-calculated densities with a coverage factor, $k = 2$.

3.2.2 Tait Viscosity Correlation

Viscosities are correlated with a Tait expression following procedures reported in our previous studies^{53, 59} and by Caudwell *et al.*⁶⁷. Equation 13 shows the Tait expression with parameters, $D(T)$ (equation 14), $E(T)$ (equation 15), and $\eta_0(T, p_0 = 0.1 \text{ MPa})$ (equation 16), which is a reference viscosity⁷⁰⁻⁷². The Tait expression is initially fit to each set of isothermal data by minimizing the Δ_{AAD} between calculated and experimental viscosities and constraining the bias to zero. The resultant parameters are then fit to equations 13 to 15. Finally, all of the parameters

found in equations 14 to 16 are refit simultaneously to the entire data set by minimizing the Δ_{AAD} and constraining the Δ_{bias} to zero. Parameters for each of the three diesels studied here are listed in Table 9 along with T - p ranges and Δ_{AAD} , Δ_{SD} , Δ_{max} , and Δ_{bias} . Figure 7 shows deviation plots comparing experimental viscosity data to Tait-calculated viscosities. The Tait-calculated viscosities are expected to have an uncertainty of 4% since 95% of the diesel viscosity data are within $\pm 4\%$.

$$\eta / mPa \cdot s = \eta_0(T) \left(\frac{p+E}{p_0+E} \right)^D \quad (13)$$

$$D = \sum_{i=0}^2 d_i (K/T)^i \quad (14)$$

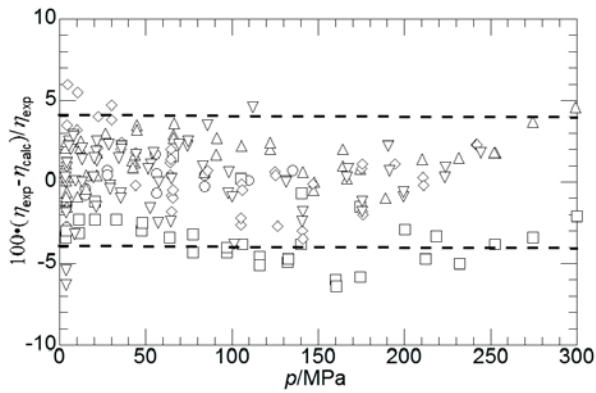
$$E / MPa = \sum_{i=0}^2 e_i (T/K)^i \quad (15)$$

$$\ln(\eta_0) = \ln(A_\eta) + \left(\frac{B_\eta}{T - C_\eta} \right) \quad (16)$$

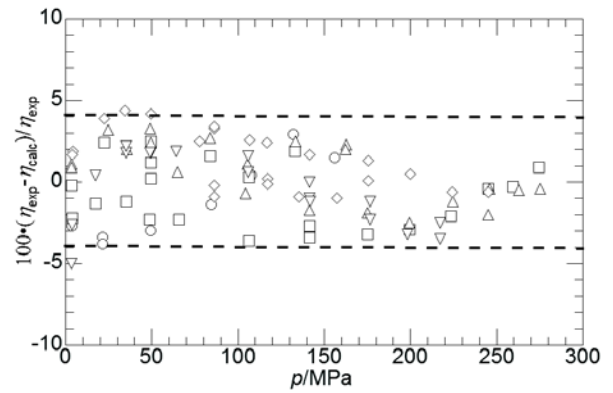
Table 9. Parameters for the Tait viscosity equation used to reproduce experimental diesel viscosities. T - p ranges, Tait parameters, Δ_{AAD} , Δ_{SD} , Δ_{max} , and Δ_{bias} are listed for the HPF, ULSD, and the HAR diesels.

	HPF	ULSD	HAR
T_{range} / K	298.3 – 528.7	298.2 – 525.4	298.4 - 532.6

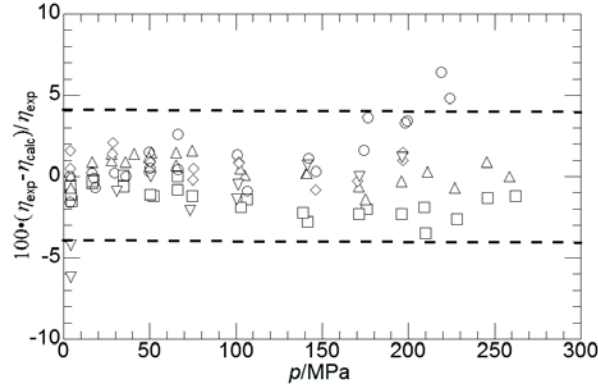
$p_{\text{range}} / \text{MPa}$	3.6 – 300.0	3.6 - 275.4	3.8 - 262.2
$10^2 \cdot A_{\eta} / \text{mPa} \cdot \text{s}$	2.4761	4.1375	3.2888
$10^{-2} \cdot B_{\eta} / \text{K}$	9.4192	7.3118	8.1391
$10^{-2} \cdot C_{\eta} / \text{K}$	1.0504	1.2663	1.1196
$10^{-1} \cdot d_0$	1.8810	1.2240	2.0257
$10^{-3} \cdot d_1 / \text{K}$	-17.229	-9.8230	-18.546
$10^{-6} \cdot d_2 / \text{K}^2$	4.2883	2.4937	4.6641
$10^{-3} \cdot e_0 / \text{MPa}$	3.7612	2.1064	4.1746
$e_1 / (\text{MPa} / \text{K})$	-14.980	-7.6343	-16.405
$10^3 \cdot e_2 / (\text{MPa} / \text{K}^2)$	15.286	7.8114	16.697
$\Delta_{\text{AAD}} / \%$	1.9	1.8	1.2
$\Delta_{\text{SD}} / \%$	1.5	1.2	1.2
$\Delta_{\text{max}} / \%$	6.4	5.2	6.4
$\Delta_{\text{bias}} / \%$	0.0	0.0	0.0



(a)



(b)



(c)

Figure 7. Experimental viscosities (η_{exp}) compared to Tait-calculated viscosities (η_{calc}) for (a) HPF, (b) ULSD, and (c) HAR diesels at approximately \circ - 300, \square - 323, \triangle - 350, \diamond - 433, and ∇ - 530 K (see Tables 5, 6, and 7 for exact temperatures). Dashed lines at $\pm 4\%$ reflect the combined expanded uncertainty for the Tait-calculated viscosities since 95% of the experimental viscosity data match calculated values to within $\pm 4\%$.

Figures 8(a) to 8(c) compare Tait-calculated viscosities from 298 to 530 K for the three diesels studied here. Each plot of the effect of pressure on viscosity is accompanied by a deviation graph showing the effect of pressure on the viscosity difference for each grouping of two diesels. A shaded box covering the region from $\pm 4\%$ shows where the grouped viscosities are within the uncertainty of the Tait correlation and, therefore, are considered indistinguishable.

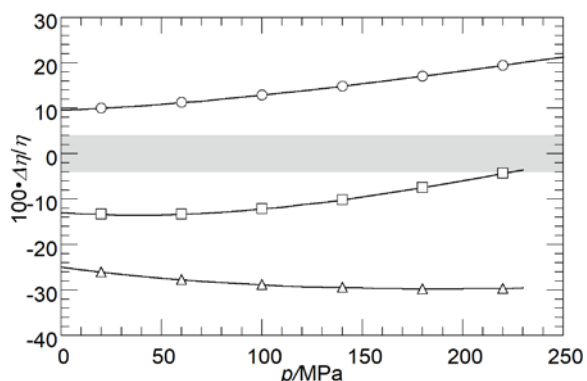
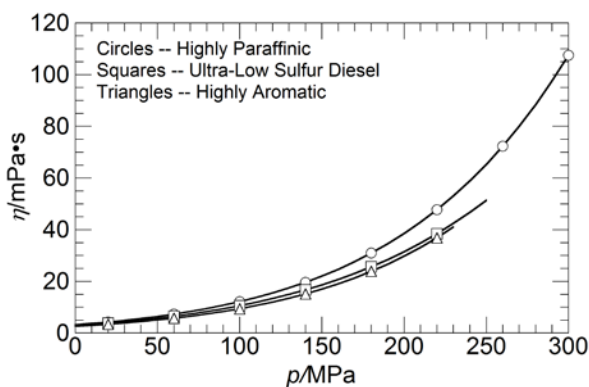
Figure 8(a) shows the viscosities at 298.2 K, which, from low to moderate pressures, scale with an increase in M_{ave} and $R_{\text{H/C}}$. HPF viscosities exhibit a positive constant offset of $\sim 22\%$ from HAR viscosities and HPF viscosities increase from ~ 10 to $\sim 20\%$ from ULSD viscosities as the pressure increases to 250 MPa. It is interesting to note that HPF has the largest viscosities, yet the lowest densities relative to HAR and ULSD. The observed HPF viscosities are likely a direct

consequence of the high isoparaffin content and greater molecular weight compared to the other two diesels.

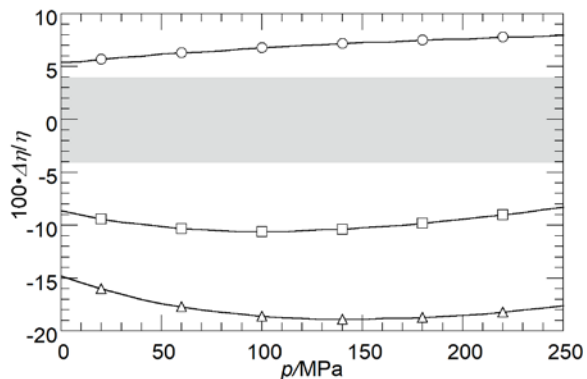
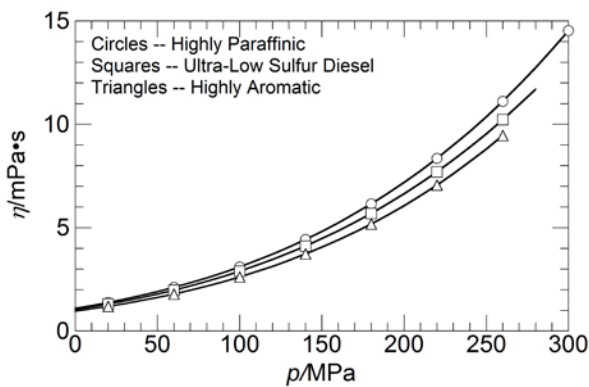
The deviation plot in Figure 8(a) also shows that HAR viscosities increase more rapidly than those for ULSD until eventually these two viscosities are within the estimated uncertainty of the Tait correlation at ~ 225 MPa. The more dramatic increase in viscosity for HAR relative to ULSD is likely a consequence of a greater concentration of naphthalenes and 3-ring aromatics that exhibit large polar interactions at this low temperature⁷³. Figure 8(b), now at 353.2 K, shows that the three sets of diesel viscosities are less sensitive with changes in pressure compared to what was observed at 298 K (note viscosity scale change in the graph) and the ULSD and HAR curves are now distinct from one another. The viscosity versus pressure graphs show that now the diesel viscosities scale with increasing M_{ave} and $R_{H/C}$ at all pressures. The deviation graph in Figure 8(b) also now shows that each grouping of two diesels exhibit constant offsets, reflecting the decreased sensitivity of the viscosities to pressure at this higher temperature. Note that Table 2 shows that there are more aromatic compounds present in both HPF and HAR relative to ULSD. Therefore, we expect HPF and HAR viscosity to be less sensitive to pressure at 353.2 K since polar interactions scale with inverse temperature⁷³. The increase in viscosity with increasing $R_{H/C}$ for the three diesels also supports this conjecture as aromatics exhibit the greatest degree of unsaturation.

Figure 8(c) shows that the viscosities of the three diesels at 530.0 K do not scale with M_{ave} and $R_{H/C}$. The accompanying deviation graph shows HPF viscosities increase at a faster rate with increasing pressure than either HAR or ULSD viscosities, but only up to a pressure to ~ 100 MPa. At higher pressures HPF viscosities then exhibit a fairly constant offset from HAR viscosities, however, ULSD viscosities now increase much faster than either HPF or HAR viscosities. Note, also, that the ULSD viscosity at the lowest pressure is $\sim 10\%$ greater than either HPF or HAR

viscosities. The high ULSD viscosity at this high temperature, where intermolecular interactions are reduced, may be related to second-order diesel composition effects, such the difference in molecular structures of the compounds within the same chemical family. The SI provides complementary viscosity figures at 323.2 and 433.0 K that show comparisons at the intermediate temperatures and reinforce the trends observed from 298.2 to 530.0 K. More HPHT viscosity studies are needed with well-defined surrogate mixtures containing differing amounts of n-paraffins, branched paraffins, and saturated cyclics and aromatics with and without linear and bulky alkyl side chains to further resolve the impact of temperature, molecular structure, and interactions on viscosity.



(a)



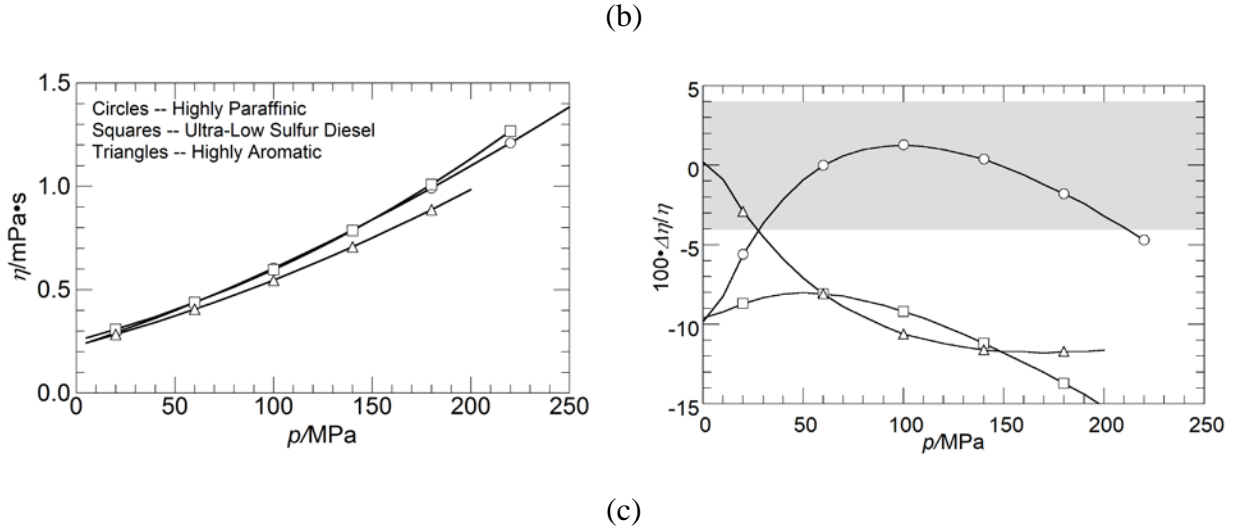


Figure 8. Comparison of Tait-calculated viscosities (lines) for three diesels at (a) 298.2, (b) 353.2 and (c) 530.0 K. Left-hand side graphs: Impact of pressure on viscosity with symbols on each line identifying a particular diesel where \triangle - HAR, \square - ULSD, and \circ - HPF; Right-hand side graphs: Deviation graph showing the effect of pressure on the difference ($100 \cdot \Delta\eta/\eta$) between sets of diesel viscosities with the symbols on each line identifying a particular set of two diesels where \circ - $100 \cdot (\eta_{\text{HPF}} - \eta_{\text{ULSD}})/\eta_{\text{HPF}}$, \square - $100 \cdot (\eta_{\text{HAR}} - \eta_{\text{ULSD}})/\eta_{\text{HAR}}$, and \triangle - $100 \cdot (\eta_{\text{HAR}} - \eta_{\text{HPF}})/\eta_{\text{HAR}}$. The gray box shows where the deviations fall within the combined expanded experimental uncertainty of the Tait-calculated viscosities with a coverage factor, $k = 2$.

3.3 Modeling

3.3.1 Pseudo-component Model for Density

Here we apply pseudo-component technique²⁰ of Rokni et al. to predict diesel densities. This technique uses the PC-SAFT EoS²² that requires as inputs the number of segments in the chain, m , the segment diameter, σ , and the strength of interaction between segments, ε/k . The three

input parameters are correlated to M_{ave} and $R_{H/C}$, which are either calculated directly knowing the mixture composition or are calculated from a chemical analysis of the mixture. For improved HPHT density predictions, Rokni and coworkers used the group contribution (GC) database of Burgess et al.⁷⁴ to create the necessary correlations. A more detailed description of the pseudo-component correlations is provided in the SI and is found elsewhere²⁰. Table 10 lists the resultant PC-SAFT EoS parameters for the three diesels studied here determined both when the M_{ave} input is M_n and M_w . Figures 9(a) to 9(c) compare the pseudo component model to select experimental data around 298, 350, and 530 K (see Tables 5, 6, and 7 for exact temperatures). The resultant Δ_{AAD} and Δ_{max} statistics in Table 10 are consistently $\sim 1\%$ lower when the PC-SAFT parameters determined using the M_w are used. The consistently positive bias and Figures 9(a) to (c) show that in all cases the pseudo-component model underpredicts the density regardless which M_{ave} value is used. However, for calculations using parameters determined using M_w are underpredicted to a lesser degree which is driven by M_w being systematically greater than M_n . Nevertheless, the pseudo-component model provides reasonable estimates for the three diesels studied here regardless of which M_{ave} is used and overall only requires a very modest amount of experimental mixture characterization data.

Table 10. Single, pseudo-component PC-SAFT parameters used to calculate the diesel densities obtained in this study²⁰.

Diesel	m	$\sigma/\text{\AA}$	$(\varepsilon/k)/\text{K}$	Δ_{AAD}	Δ_{bias}	Δ_{SD}	Δ_{max}
M_n							
HPF	8.755	3.400	254.5	2.1	2.1	0.5	2.9
ULSD	8.308	3.395	253.8	3.1	3.1	0.6	4.9

HAR	8.116	3.389	258.2	2.1	2.1	0.6	3.5
M_w							
HPF	9.239	3.405	256.6	1.3	1.3	0.4	2.2
ULSD	8.748	3.400	256.0	2.3	2.3	0.6	3.9
HAR	8.428	3.394	260.1	1.4	1.4	0.6	2.8

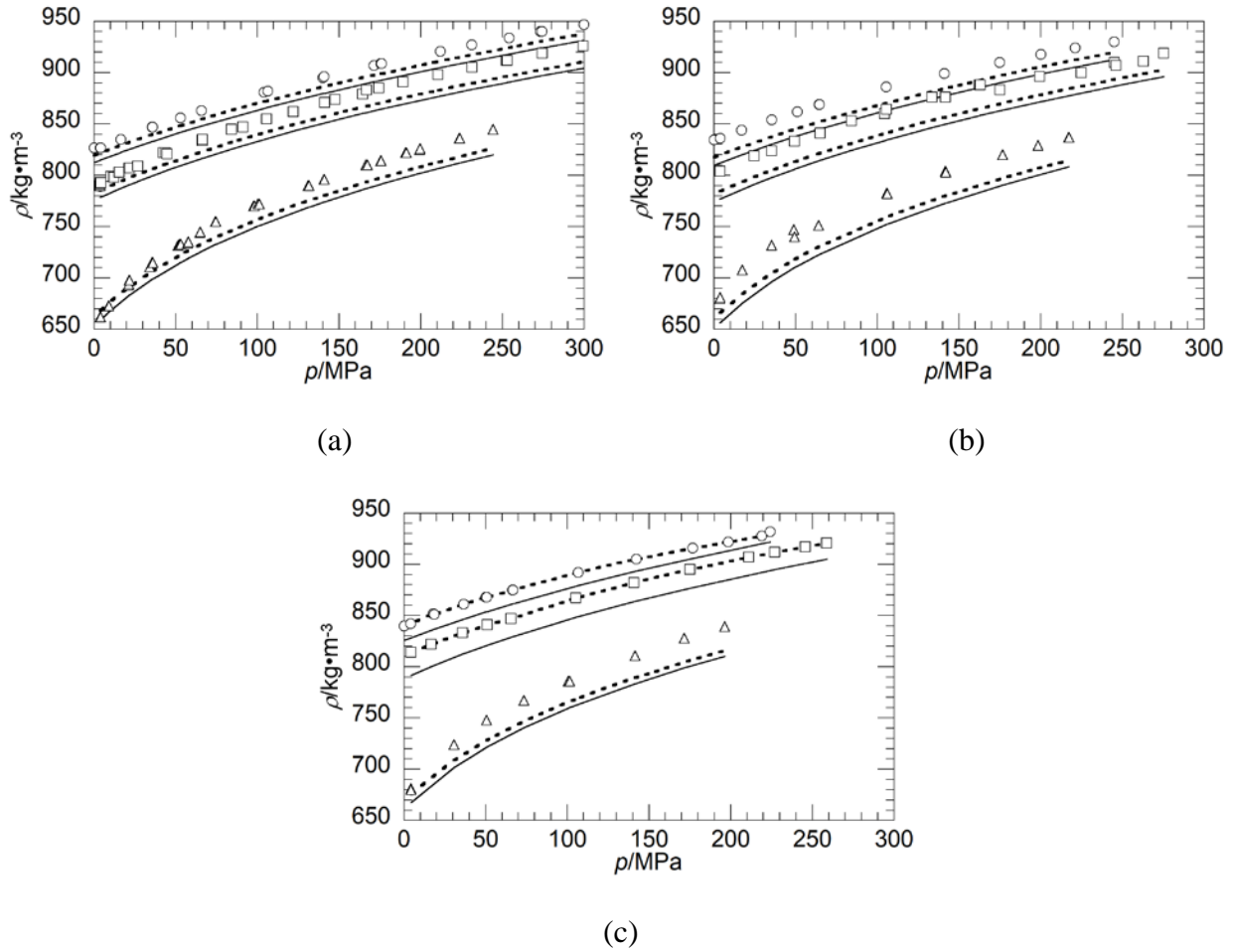


Figure 9. Comparison of experimental density data to the pseudo-component model of Rokni et al. for (a) HPF, (b) ULSD, and (c) HAR. Symbols represent data points at select isotherms around \circ - 298, \square - 350, and \triangle - 529 K (see Tables 5, 6, and 7 for exact temperatures).

Solid and dashed lines represent predictions using parameters determined using the number average molecular weight, M_n , and weight average molecular weight, M_w , respectively.

Figure 10 presents performance details for the single, pseudo-component model of Rokni et al. for density predictions at 298.0 K for the three diesels studied here where the parameters are calculated using only M_w . Identical trends are observed for calculations using M_n and temperatures greater than 298.0 K and therefore are not shown here. The results in these figures are predicted curves only and not comparisons to experimental data. Figure 10(a) shows the variation in the densities with pressure predicted using pseudo-component method of Rokni et al. Figure 10(b) is a companion deviation graph showing the effect of pressure on the density difference between each grouping of two diesels. In this instance the HAR diesel exhibits the greatest density, consistent with the experimental data. However, ULSD densities are predicted to be the least dense of the three diesels, which is inconsistent with the trend at low pressure conditions. Additionally, Figure 10(b) shows that the pseudo-component model does not replicate the effect of pressure on the density difference between the different groupings of diesels shown in Figure 6(b). Identical trends are found with this model at all temperatures greater than 298 K and, therefore, are not shown here. Although Rokni's pseudo-component method provides very reasonable predictions for diesel densities, it is not unexpected that this single, pseudo-component method does not predict the influence of the molecular weight and chemical family distribution in the diesels that cause density variations with increasing pressure.

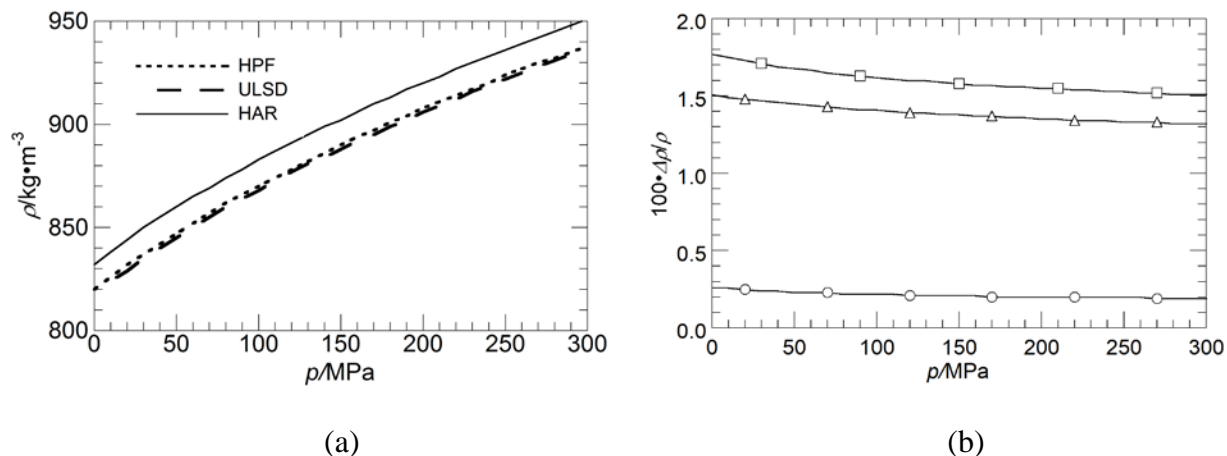


Figure 10. Densities at 298.0 K calculated using Rokni's²⁰ model where parameters are determined using the weight average molecular weight, M_w . (a) Calculated pressure effect. (b) Deviation graph showing the calculated effect of pressure on the difference ($100 \cdot \Delta\rho/\rho$) between sets of diesel densities with the symbols on each line identifying a particular set of two diesels where \circ - $100 \cdot (\rho_{\text{HPF}} - \rho_{\text{ULSD}})/\rho_{\text{HPF}}$, \square - $100 \cdot (\rho_{\text{HAR}} - \rho_{\text{ULSD}})/\rho_{\text{HAR}}$, and \triangle - $100 \cdot (\rho_{\text{HAR}} - \rho_{\text{HPF}})/\rho_{\text{HAR}}$.

3.3.2 Pseudo-component Model for Viscosity

Rokni et al.⁴⁵ also developed a facile pseudo-component technique for viscosity predictions based on the observation that reduced viscosity scales with reduced entropy⁷⁵. This observation was developed into a calculation methodology by Novak^{76,77} and further generalized by Lötgering-Lin and Gross⁴⁶ who use the PC-SAFT EoS²² with a GC method for calculating the viscosity correlation coefficients needed to predict viscosity. Here we provide a brief overview of Rokni et al.'s technique and direct the reader to the SI and elsewhere⁴⁵ for additional details. In this instance, Rokni and coworkers maintain internal consistency of their approach by using GC parameters of Sauer et al.⁷⁸ to develop the correlations needed to calculate m , σ , and ε/k for the pseudo-

component rather than using Burgess's GC parameters.⁷⁴ The PC-SAFT EoS is now used to calculate the reduced entropy needed to correlate to viscosity. Rokni and coworkers integrated the single, pseudo-component approach with the GC approach of Lötgering-Lin and Gross to create correlations to predict the four parameters needed with the reduced entropy-viscosity correlation. Rokni et al. show how these four parameters are correlated to the mixture M_{ave} and $R_{H/C}$. Rokni and coworkers⁴⁵ also show that in many cases single, pseudo-component viscosity predictions can be improved if one of the four GC-calculated, viscosity parameters is fit to a single viscosity data point at a reference state, which here is 298.15 K and 0.1 MPa. In the previous study by Rokni et al. the performance of the pseudo-component was only tested when M_n was used as the M_{ave} input to the pseudo-component model. However, here the performance of the pseudo-component model is compared when using both M_n and M_w .

Table 11 lists the resultant PC-SAFT EoS parameters for the three diesels calculated using both M_n and M_w , which are very different than those shown in Table 10 calculated with Burgess's GC method. Table 11 also lists values for A , B , C , D , and D^{fit} (fit to a single viscosity data point) determined with M_n and M_w which are used with the viscosity correlation detailed in the SI and elsewhere⁴⁵. Figures 11(a) to 11(c) compare the performance of the pseudo-component model of Rokni et al. when M_n and M_w molecular weight averages are used for both model variations. The left-hand side images in Figures 11(a) to 11(c) show that calculations for all three diesels using both M_n and M_w underpredict the viscosity at 298 and 350 K and over predict the viscosity at 530 K. However, predictions using M_w to calculate the model parameters results superior predictions at low temperature and predictions using M_n more accurately depict the experimental data at high-temperatures. On the right-hand side in Figures 11(a) to 11(c) show that the degree to which the viscosities are underpredicted can be reduced if the parameter D is a fitted parameter. Figures 12(a)

and 12(b) compare how much the performance of the entropy scaling model can be improved when D is a fitted parameter for calculations incorporating parameters determined with M_n and M_w , respectfully. Figure 12(a) shows that if M_n is used to determine the model parameters a dramatic improvement in the Δ_{AAD} is observed when incorporating D^{fit} . Conversely, Figure 12(b) shows that if M_w is used to calculate model parameters using D^{fit} results in no significant improvement to the overall Δ_{AAD} . The result is likely result of the reduced sensitivity of the parameter D in relation to the other entropy scaling coefficients A , B , and C when M_w is used in place of M_n . It can be seen in Table 11 that parameters A , B , and C determined using M_w are consistently greater than those determined using M_n

Table 11. Single, pseudo-component PC-SAFT parameters used to calculate diesel viscosities obtained in this study⁴⁵.

Diesel	m	$\sigma/\text{\AA}$	$(\varepsilon/k)/\text{K}$	A	B	C	D	D^{fit}
M_n								
HPF	6.493	3.848	249.2	-0.808	-3.677	-0.759	-0.178	-0.210
ULSD	6.138	3.845	249.6	-0.790	-3.571	-0.725	-0.169	-0.204
HAR	5.999	3.839	253.3	-0.774	-3.531	-0.718	-0.167	-0.209
M_w								
HPF	6.884	3.849	249.6	-0.827	-3.793	-0.798	-0.190	-0.202
ULSD	6.500	3.847	250.1	-0.807	-3.679	-0.761	-0.179	-0.196
HAR	6.259	3.841	253.9	-0.785	-3.611	-0.744	-0.175	-0.176

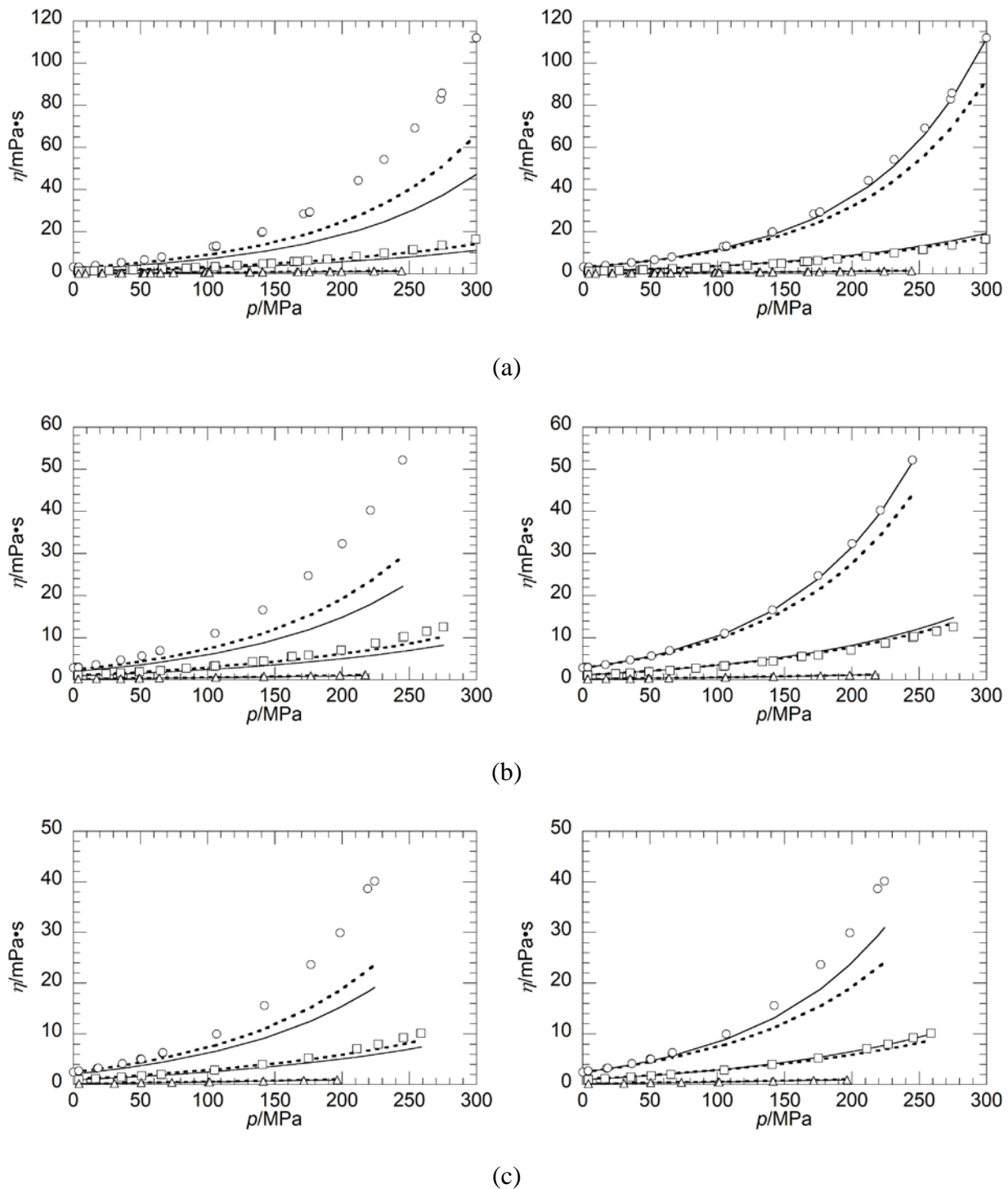


Figure 11. Comparison of experimental viscosity data to the pseudo-component model of Rokni et al. for (a) HPF, (b) ULSD, and (c) HAR. Symbols represent data points at select isotherms around \circ - 298, \square - 350, and \triangle - 529 K (see Tables 5, 6, and 7 for exact

temperatures). Solid and dashed lines represent predictions using parameters determined using the number average molecular weight, M_n , and weight average molecular weight, M_w , respectively. Left-hand and right-hand figure represent predictions where the parameter D is a calculated value and D is fit to a single viscosity data point at 298.15 K and 0.1 MPa, respectively.

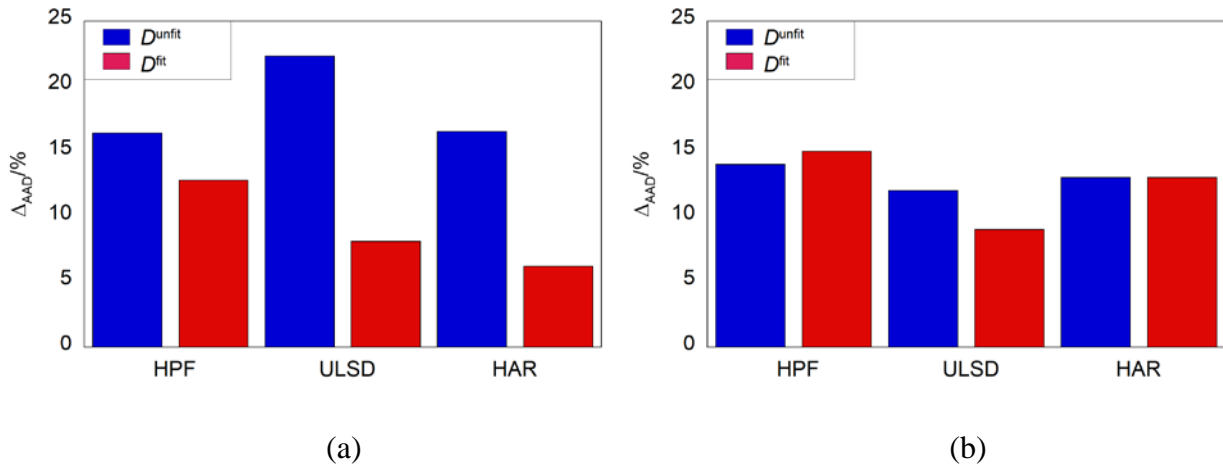
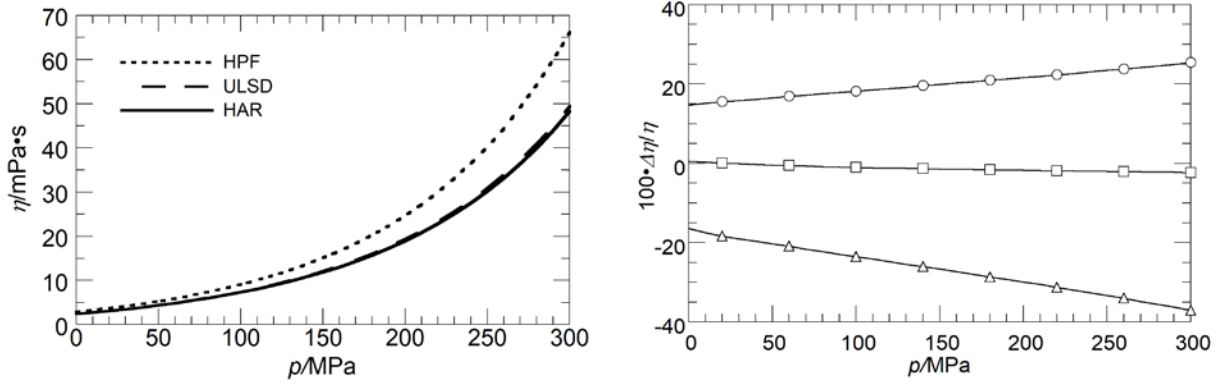


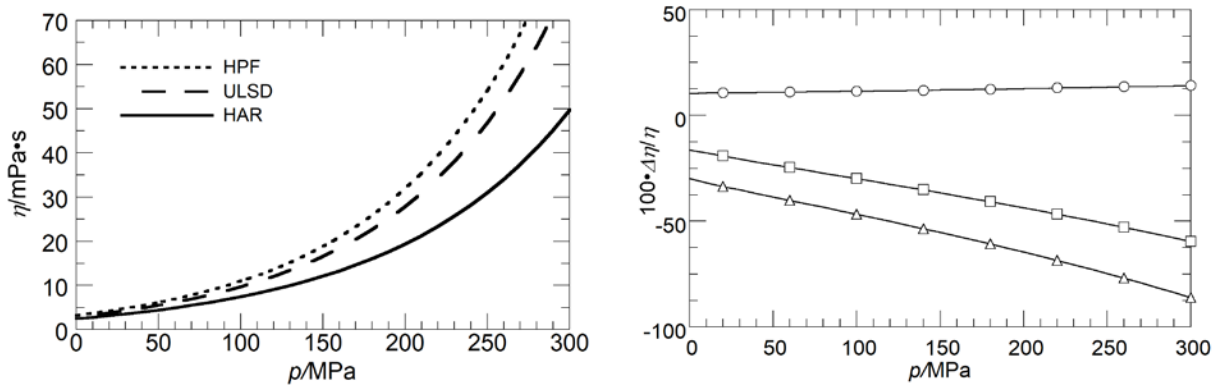
Figure 12. Performance of the viscosity pseudo-component model of Rokni et al. characterized with the Δ_{AAD} where pseudo-component parameters are determined using (a) the number average molecular weight, M_n , or (b) the mass average molecular weight, M_w .

Figures 13(a) and 13(b) present performance details for Rokni et al.'s single, pseudo-component method for viscosity predictions at 298.2 K where the experimental viscosities of the three diesels varied non-monotonically with pressure. The results in these graphs are predicted curves only and not comparisons to experimental data and they only show results for calculations using parameters determined from M_w . Predictions where parameters are determined using M_n are provided in the SI. Each plot of the effect of pressure on viscosity is accompanied by a deviation

graph showing the effect of pressure on the viscosity difference between each grouping of two diesels. Figures 13(a) and 13(b) show that both variations of the model predict that viscosity and the rate of viscosity increase scale with increasing M_w and $R_{H/C}$. However, ULSD and HPF viscosities calculated with appropriate D^{fit} values are now distinctly different, which is still not in agreement with observed experimental behavior. While the single, pseudo-component model provides reasonable viscosity predictions it does not accurately depict the experimentally observed viscosity increase with pressure shown in Figure 8(a). The companion deviation graphs in Figures 13(a) and 13(b) show that ULSD and HAR viscosities diverge with increasing pressure rather than converge at high pressures, as seen experimentally in Figure 8(a). The predicted deviation curves in Figure 13(a) and 13(b) exhibit monotonic responses to pressure rather than the nonmonotonic responses experimentally observed. It is expected that these non-monotonic responses are more closely related to second order effects controlled by the molecular weight distribution of the diesel. The strength of this model is that only a limited amount of diesel characterization information is needed to obtain very reasonable predictions of HPHT viscosities. At present the single, pseudo-component model, nor to the best of our knowledge any other model, is capable of predicting the impact of second-order diesel composition effects, such as the overall molecular weight distribution, the dispersion of molecular weights within individual chemical families, and the differences in molecular structure of compounds within the same chemical family.



(a)



(b)

Figure 13. Predicted effect of pressure on viscosity at 298.2 K calculated using the pseudo-component method of Rokni et al. where (a) D is calculated using the model correlation and (b) D is fit to viscosity data at 298.15 K and 0.1 MPa. Left-hand side graphs: Impact of pressure on viscosity; Right-hand side graphs: Deviation graph showing the effect of pressure on the difference ($100 \cdot \Delta\eta/\eta$) between sets of diesel viscosities with the symbols on each line identifying a particular set of two diesels where \circ - $100 \cdot (\eta_{\text{HPF}} - \eta_{\text{ULSD}}) / \eta_{\text{HPF}}$, \square - $100 \cdot (\eta_{\text{HAR}} - \eta_{\text{ULSD}}) / \eta_{\text{HAR}}$, and \triangle - $100 \cdot (\eta_{\text{HAR}} - \eta_{\text{HPF}}) / \eta_{\text{HAR}}$.

3.3.3 Free Volume Theory for Viscosity

Here the Free Volume Theory (FVT) model is used to characterize the HPHT viscosity data obtained in this study. FVT is composed of a dilute gas viscosity, η_0 calculated from the kinetic theory of gases (equation 17), and a residual term, $\Delta\eta$ (equation 18).⁷⁹

$$\eta/\text{mPa} \cdot \text{s} = \eta_0 + \Delta\eta \quad (17)$$

$$\Delta\eta/\text{mPa} \cdot \text{s} = \frac{\rho L \left(\alpha \rho + \frac{\rho M_w}{\rho} \right)}{\sqrt{3RT} M_{\text{ave}}} \exp \left[B_v \left(\frac{\alpha \rho + \frac{\rho M_w}{\rho}}{RT} \right)^{3/2} \right] \quad (18)$$

where ρ is calculated using the PC-SAFT EoS with parameters calculated using the density pseudo-component model where parameters are determined using M_w , and R is the universal gas constant. Table 12 lists the three FVT parameters, L (Å), α ($\text{m}^5 \cdot \text{mol}^{-1} \cdot \text{s}^{-2}$), and B_v (dimensionless), regressed against the entire set of experimental viscosities. Here the goal is to determine whether FVT parameters can be correlated to M_w and $R_{H/C}$ analogous to the approach used with the single, pseudo-component method⁴⁵. Therefore, in addition to the viscosity data reported here, we include the viscosity data of Aquino and coworkers⁷ for Highly Naphthenic (HNAP) and Middle East Straight Run (MESR) diesels to create a larger sample set of FVT parameters as shown in Table 12.

Table 12. Diesel characterization information, $R_{H/C}$, M_{ave} , and FVT parameters L , α , and B_v optimized by fitting diesel viscosity data obtained in this study and data reported by Aquino et al.⁷ Densities needed for FVT predictions are calculated with the PC-SAFT EoS using

parameters fit to HPHT densities for each diesel. The performance of FVT is characterized by the Δ_{AAD} and Δ_{max} .

Diesel	$R_{H/C}$	$M_w/g \cdot mol^{-1}$	$L/\text{\AA}$	$\alpha/m^5 \cdot mol^{-1} \cdot s^{-2}$	$B_v \cdot 10^3$	$\Delta_{AAD}/\%$	$\Delta_{max}/\%$
HPF	1.91	212.0	0.6300	186.9	5.5334	7	30
ULSD	1.89	199.9	0.6239	190.1	5.3393	7	27
HAR	1.81	194.5	0.5738	171.4	6.1152	7	27
HNAP	1.74	221.2	0.3984	220.5	5.0159	6	27
MESR	1.85	235.7	0.2827	274.3	4.1831	7	17

Figure 14 shows that the fitted FVT parameters L and B_v vary linearly with M_{ave} , and α varies linearly with the $M_{ave} \cdot R_{H/C}^{-0.1530}$. L , α , and B_v are fit to Equations 19 to 21 with optimized parameters listed in Table 13. In order to obtain the best fit of all five sets of diesel viscosities, parameters l_1 , l_0 , a_1 , a_0 , n , b_1 , and b_0 are re-optimized by minimizing the collective Δ_{AAD} and constraining Δ_{bias} to a value of zero. Table 14 lists the re-optimized parameters for equations 19 to 21. Modest improvements in viscosity predictions are seen in the Δ_{AAD} for each diesel and the collective Δ_{AAD} for all diesels.

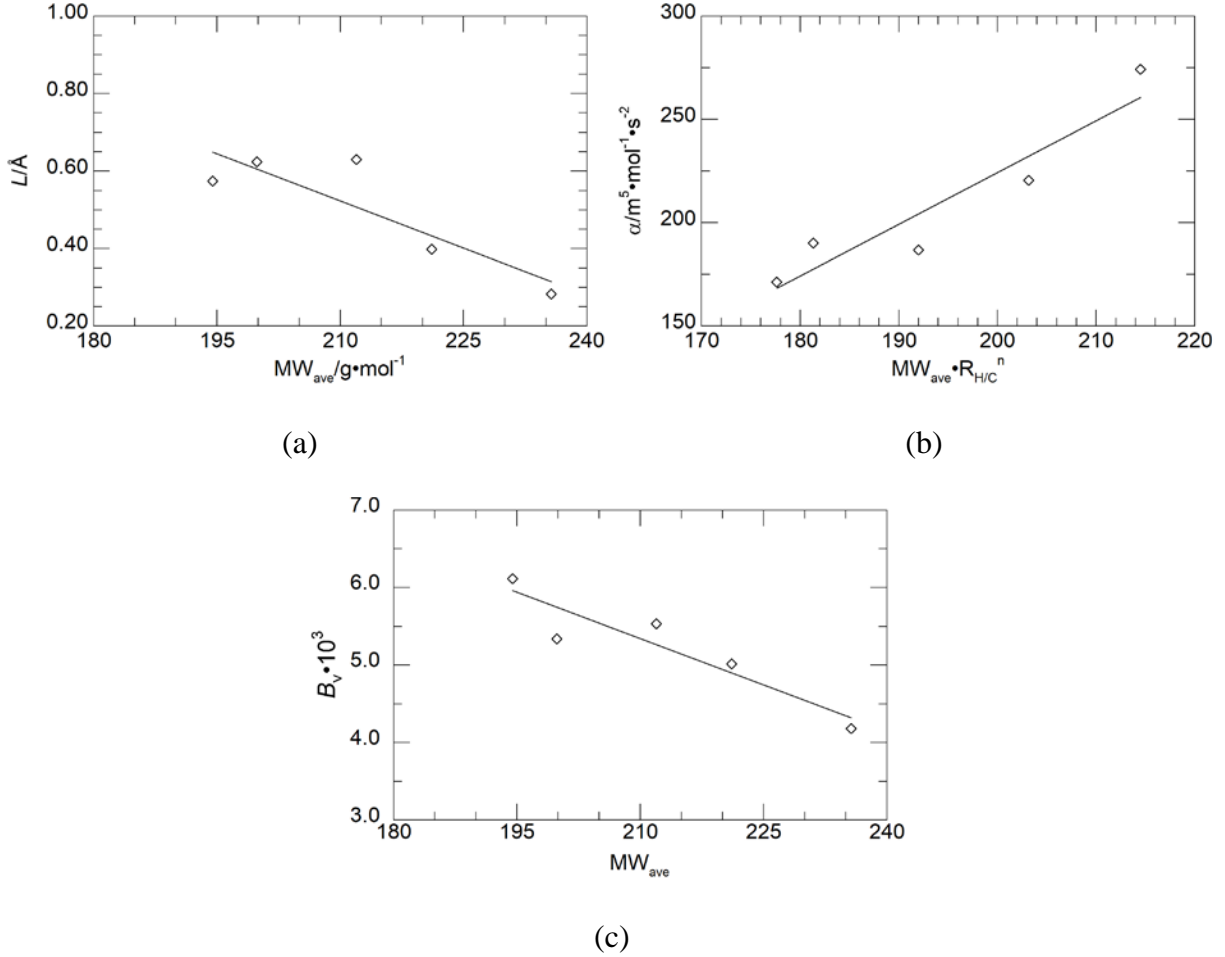


Figure 14. Correlations between FVT parameters L , α , and B_v and basic compositional information.

(a) Relationship between L and M_{ave} and (b) Relationship between α and $M_{ave}\cdot R_{H/C}^n$ where $n = -0.1530$ and (c) Linear relationship between B_v and M_{ave} .

$$L/\text{\AA} = l_1 M_{ave} + l_0 \quad (19)$$

$$\alpha/\text{m}^5 \cdot \text{mol}^{-1} \cdot \text{s}^{-2} = a_1 M_{ave} \cdot R_{H/C}^n + a_0 \quad (20)$$

$$B_v = b_1 M_{ave} + b_0 \quad (21)$$

Table 13. Coefficients needed to calculate FVT parameters L , α , and B_v from M_w and $R_{H/C}$ using the linear correlations shown in equations 17 to 19. Densities needed for the FVT predictions are calculated with the PC-SAFT EoS using parameters fit to HPHT densities for each diesel. The performance of FVT is characterized by the Δ_{AAD} and Δ_{max} for each diesel and for all five diesels collectively.

$L/\text{\AA}$		$\alpha/\text{m}^5\cdot\text{mol}^{-1}\cdot\text{s}^{-2}$		B_v		
l_1	l_0	a_1	a_0	b_1	b_0	n
$-8.1011\cdot 10^{-3}$	2.2244	2.5010	-275.9	$-3.9800\cdot 10^{-5}$	$1.3701\cdot 10^{-2}$	-0.1530
	HPF	ULSD	HAR	HNAP	MESR	Overall
$\Delta_{AAD}/\%$	9	12	7	31	8	11
$\Delta_{MAX}/\%$	45	34	34	54	24	54

Table 14. Re-optimized coefficients needed to calculate FVT parameters L , α , and B_v from M_w and $R_{H/C}$ using equations 17 to 19. Densities needed for the FVT predictions are calculated with the PC-SAFT EoS using parameters fit to HPHT densities for each diesel. The performance of FVT is characterized by the Δ_{AAD} and Δ_{max} for each diesel and all five diesels collectively.

$L/\text{\AA}$		$\alpha/\text{m}^5\cdot\text{mol}^{-1}\cdot\text{s}^{-2}$		B_v		
l_1	l_0	a_1	a_0	b_1	b_0	n
$-1.3868\cdot 10^{-3}$	0.8494	0.83805	-12.731	$-2.1797\cdot 10^{-5}$	$9.9108\cdot 10^{-3}$	0.2790
	HPF	ULSD	HAR	HNAP	MESR	Overall

$\Delta_{AAD}/\%$	8	7	8	7	10	8
$\Delta_{MAX}/\%$	28	27	31	36	29	36

Although the performance of the FVT model is comparable to that of the previously described, single, pseudo-component model, the correlations used to calculate FVT parameters may only be applicable over the narrow M_w range studied here and, therefore, cannot be considered purely predictive. To use the FVT model in a purely predictive mode a group contribution database is needed to estimate L , α , and B_v for various hydrocarbons relevant to those found in diesel fuel.

4. Conclusions

Densities and viscosities are measured with an RBVD for three diesels at temperatures from 298.2 to 532.6 K and pressures up to 300.0 MPa. A universal calibration procedure for the RBVD used here for complex multicomponent mixtures shows that the reference calibration constant, K_0 , agrees reasonably well with experimentally determined values for the HPF and HAR diesels, but deviates from that for the ULSD diesel. Nevertheless, this universal calibration procedure can still be used to calculate a reference calibration constant when accurate ambient pressure density and viscosity data are available. More work is in progress to extend the range of this calibration equation to a wide range of chemical compounds, including saturated cyclics and branched aromatics, which may influence the resultant fluid dependent calibration parameter, K_0 .

Although the trends in the observed HPHT densities and viscosities can be related to the chemical composition of the diesels, we speculate that many of these trends are related to second-order diesel composition effects, such as the overall molecular weight distribution, the dispersion of molecular weights within individual chemical families, and the differences in chemical structure

within the same chemical family. Further fundamental HPHT viscosity studies are needed with well-characterized surrogate mixtures with varying amounts of normal and branched paraffins, and cyclics and aromatics with linear and bulky side chains to ascertain the impact of non-paraffinic compounds on HPHT diesel fluid properties.

A single, pseudo-component model, using only M_{ave} and $R_{H/C}$ as input, also provides a straightforward, yet powerful, method to calculate reasonable values for HPHT densities and viscosities. However, the single, pseudo-component model does not capture the non-monotonic variations in density and viscosity with increasing pressure observed in this study. We expect these trends are more closely controlled by the carbon number dispersion of individual chemical families, and the variation of chemical structure within a specific chemical family. The FVT model, with parameters calculated in terms of diesel M_{ave} and $R_{H/C}$, provides a reasonable representation of HPHT viscosity data. Although this correlation works well with five different diesel fuels considered here, further development is needed to be a purely predictive model.

Supporting Information

The supplemental information contains data tables listing the carbon number and corresponding weight percent of each chemical family for each diesel studied here, density-pressure plots developed with the Tait equation, a detailed description of the pseudo-component model applied to density predictions and the model applied to viscosity predictions, PC-SAFT parameters needed to calculate viscosities with the Free Volume Theory model.

Acknowledgments

This project has received funding from the European Union Horizon 2020 Research and Innovation program, Grant Agreement No 675528. The authors thank Joseph Roos (Afton), Joseph Remias (Afton), Mark Devlin (Afton), and Rajendar Reddy Mallepally (VCU) for their helpful, technical discussions. We also thank Cheyenne Urbine (Afton) and Kevin Layton (Afton) for providing ambient pressure viscosity and density information measured using the Stabinger viscometer.

References

1. Fitzgibbon, T.; Ding, C.; Szabat, P. Diesel demand: still growing globally despite Dieselgate. <https://www.mckinsey.com/industries/oil-and-gas/our-insights/petroleum-blog/diesel-demand-still-growing-globally-despite-dieselgate> (26 June 2019),
2. Diesel has a future: Diesel's new ecological efficiency. <https://www.bosch-mobility-solutions.com/en/highlights/powertrain-and-electrified-mobility/the-future-of-diesel/> (26 June 2019),
3. Griffin, J.; Fantini, A.-M., World Oil Outlook 2040. Organization of the Petroleum Exporting Countries: Vienna, Austria, 2017.
4. Johnson, J. E.; Yoon, S. H.; Naber, J. D.; Lee, S.-Y.; Hunter, G.; Truemner, R.; Harcombe, T., Characteristics of 3000 bar diesel spray injection under non-vaporizing and vaporizing conditions. In *International Conference on Liquid Atomization and Spray Systems*, Heidelberg, Germany, 2012.
5. Crua, C.; Manin, J.; Pickett, L. M., On the transcritical mixing of fuels at diesel engine conditions. *Fuel* **2017**, 208, 535-548.
6. Salemi, R.; Koukouvinis, P.; Strotos, G.; McDavid, R.; Wang, L.; Li, J.; Marengo, M.; Gavaises, M., Evaluation of friction heating in cavitating high pressure diesel injector nozzles. *J Phys: Conf Ser* **2015**, 656, 012083.
7. Aquino, M.; Ciotta, F.; Creton, B.; Féjean, C.; Pina, A.; Dartiguelongue, C.; Trusler, J. P. M.; Vignais, R.; Lugo, R.; Ungerer, P., Composition analysis and viscosity prediction of complex fuel mixtures using a molecular-based approach. *Energy Fuels* **2012**, 26, 2220-2230.

8. Bair, S., The pressure and temperature dependence of volume and viscosity of four diesel fuels. *Fuel* **2014**, 135, 112-119.
9. Duncan, A. M.; Aghosseini, A.; McHenry, R.; Depcik, C. D.; Stagg-Williams, S. M.; Scurto, A. M., High-pressure viscosity of biodiesel from soybean, canola, and coconut oils. *Energy Fuels* **2010**, 24, 5708-5716.
10. Schaschke, C.; Fletcher, I.; Glen, N., Density and viscosity measurement of diesel fuels at combined high pressure and elevated temperature. *Processes* **2013**, 1, 30-48.
11. Kwak, T.; Mansoori, G., Van der Waals mixing rules for cubic equations of state. Applications for supercritical fluid extraction modelling. *Chem Eng Sci* **1986**, 41, 1303-1309.
12. Van der Waals, J. D. On the continuity of the gas and liquid state. Doctoral Dissertation, Leiden, 1873.
13. Jamaluddin, A.; Kalogerakis, N.; Chakma, A., Predictions of CO₂ solubility and CO₂ saturated liquid density of heavy oils and bitumens using a cubic equation of state. *Fluid Phase Equilib* **1991**, 64, 33-48.
14. Nikookar, M.; Omidkhah, M.; Pazuki, G., Prediction of density and solubility parameter of heavy oils and SARA fractions using cubic equations of state. *Petrol Sci Technol* **2008**, 26, 1904-1912.
15. Peng, D.-Y.; Robinson, D. B., A new two-constant equation of state. *Ind Eng Chem Fundam* **1976**, 15, 59-64.
16. Pratas, M. J.; Oliveira, M. B.; Pastoriza-Gallego, M. J.; Queimada, A. J.; Pineiro, M. M.; Coutinho, J. A., High-pressure biodiesel density: experimental measurements, correlation,

- and cubic-plus-association equation of state (CPA EoS) modeling. *Energy Fuels* **2011**, *25*, 3806-3814.
17. Soave, G., Equilibrium constants from a modified Redlich-Kwong equation of state. *Chem Eng Sci* **1972**, *27*, 1197-1203.
 18. Elliott Jr, J. R.; Suresh, S. J.; Donohue, M. D., A simple equation of state for non-spherical and associating molecules. *Ind Eng Chem Eng* **1990**, *29*, 1476-1485.
 19. Oliveira, M. B.; Freitas, S. V.; Llovell, F.; Vega, L. F.; Coutinho, J. A., Development of simple and transferable molecular models for biodiesel production with the soft-SAFT equation of state. *Chem Eng Res Des* **2014**, *92*, 2898-2911.
 20. Rokni, H. B.; Gupta, A.; Moore, J. D.; M^cHugh, M. A.; Bamgbade, B. A.; Gavaises, M., Purely predictive method for density, compressibility, and expansivity for hydrocarbon mixtures and diesel and jet fuels up to high temperatures and pressures. *Fuel* **2019**, *236*, 1377-1390.
 21. Abutaqiya, M. I.; Panuganti, S. R.; Vargas, F. M., Efficient algorithm for the prediction of PVT properties of crude oils using the PC-SAFT EoS. *Ind Eng Chem Res* **2017**, *56*, 6088-6102.
 22. Gross, J.; Sadowski, G., Perturbed-chain SAFT: An equation of state based on a perturbation theory for chain molecules. *Ind Eng Chem Res* **2001**, *40*, 1244-1260.
 23. Gil-Villegas, A.; Galindo, A.; Whitehead, P. J.; Mills, S. J.; Jackson, G.; Burgess, A. N., Statistical associating fluid theory for chain molecules with attractive potentials of variable range. *J Chem Phys* **1997**, *106*, 4168-4186.

24. Lympieriadis, A.; Adjiman, C. S.; Galindo, A.; Jackson, G., A group contribution method for associating chain molecules based on the statistical associating fluid theory (SAFT- γ). *J Chem Phys* **2007**, 127, 234903.
25. Lin, R.; Tavlarides, L. L., Thermophysical properties needed for the development of the supercritical diesel combustion technology: Evaluation of diesel fuel surrogate models. *J Supercrit Fluids* **2012**, 71, 136-146.
26. Benedict, M.; Webb, G. B.; Rubin, L. C., An empirical equation for thermodynamic properties of light hydrocarbons and their mixtures I. Methane, ethane, propane and *n*-butane. *J Chem Phys* **1940**, 8, 334-345.
27. Vidal, A.; Rodriguez, C.; Koukouvinis, P.; Gavaises, M.; M^cHugh, M. A., Modelling of diesel fuel properties through its surrogates using Perturbed-Chain, Statistical Associating Fluid Theory. *Int J Eng Res* **2018**, 1468087418801712.
28. Tihic, A.; Kontogeorgis, G. M.; von Solms, N.; Michelsen, M. L.; Constantinou, L., A predictive group-contribution simplified PC-SAFT equation of state: application to polymer systems. *Ind Eng Chem Res* **2008**, 47, 5092-5101.
29. Kontogeorgis, G. M.; Folas, G. K., *Thermodynamic models for industrial applications: from classical and advanced mixing rules to association theories*. John Wiley & Sons: West Sussex, United Kingdom, 2009.
30. Liang, X., Yan, W., Thomsen, K., Kontogeorgis, G.M., On petroleum fluid characterization with the PC-SAFT equation of state. *Fluid Phase Equilib* **2014**, 375, 254-268.
31. Yarranton, H. W., Satyro, M.A., Expanded fluid-based viscosity correlation for hydrocarbons. *Ind Eng Chem Res* **2009**, 48, 3640-3648.

32. Motahhari, H., Satyro, M.A., Taylor, S.D., Yarranton, H.W., Extension of the expanded fluid viscosity model to characterized oils. *Energy Fuels* **2013**, 27, 1881-1898.
33. Motahhari, H., Schoeggl, F., Satyro, M., Yarranton, H., Viscosity prediction for solvent-diluted live bitumen and heavy oil at temperatures up to 175-deg-C. *J Can Petrol Technol* **2013**, 52, 376-390.
34. Ma, M., Chen, S., Abedi, J., Modeling the density, solubility and viscosity of bitumen/solvent systems using PC-SAFT. *J Petrol Sci Eng* **2016**, 139, 1-12.
35. Quiñones-Cisneros, S. E.; Zéberg-Mikkelsen, C. K.; Stenby, E. H., The friction theory (f-theory) for viscosity modeling. *Fluid Phase Equilib* **2000**, 169, 249-276.
36. Quiñones-Cisneros, S. E.; Zéberg-Mikkelsen, C. K.; Baylaucq, A.; Boned, C., Viscosity modeling and prediction of reservoir fluids: From natural gas to heavy oils. *Int J Thermophys* **2004**, 25, 1353-1366.
37. Quiñones-Cisneros, S. E.; Dalberg, A.; Stenby, E. H., PVT characterization and viscosity modeling and prediction of crude oils. *Petrol Sci Technol* **2004**, 22, 1309-1325.
38. Schmidt, K. A.; Quiñones-Cisneros, S. E.; Kvamme, B., Density and viscosity behavior of a north sea crude oil, natural gas liquid, and their mixtures. *Energy Fuels* **2005**, 19, 1303-1313.
39. Abutaqiya, M. I.; Zhang, J.; Vargas, F. M., Viscosity modeling of reservoir fluids using the Friction Theory with PC-SAFT crude oil characterization. *Fuel* **2019**, 235, 113-129.
40. Khoshnamvand, Y. A., M., Viscosity prediction for petroleum fluids using free volume theory and PC-SAFT. *Int J Thermophys* **2018**, 39, 54.

41. Sun, Y.; Shen, G.; Held, C.; Lu, X.; Ji, X., Modeling viscosity of ionic liquids with electrolyte Perturbed-Chain Statistical Associating Fluid Theory and Free Volume Theory. *Ind Eng Chem Res* **2018**, *57*, 8784-8801.
42. Assael, M. J.; Dymond, J. H.; Tselekidou, V., Correlation of high-pressure thermal conductivity, viscosity, and diffusion coefficients for *n*-alkanes. *Ind Eng Chem Res* **1990**, *11*, 863-873.
43. Dymond, J. H., Awan, M.A., Correlation of high-pressure diffusion and viscosity coefficients for *n*-alkanes. *Int J Thermophys* **1989**, *10*, 941-951.
44. Ijaz, F. Measurement and prediction of the viscosity of hydrocarbon mixtures and crude oils. Imperial College, London, 2011.
45. Rokni, H. B.; Moore, J. D.; Gupta, A.; M^cHugh, M. A.; Gavaises, M., Entropy scaling based viscosity predictions for hydrocarbon mixtures and diesel fuels up to extreme conditions. *Fuel* **2019**, *241*, 1203-1213.
46. Lötgering-Lin, O.; Gross, J., Group contribution method for viscosities based on entropy scaling using the perturbed-chain polar statistical associating fluid theory. *Ind Eng Chem Res* **2015**, *54*, 7942-7952.
47. Macias-Salinas, R., Durán-Valencia, C., López-Ramírez, S., Bouchot, C., Eyring-theory-based model to estimate crude oil viscosity at reservoir conditions. *Energy Fuels* **2008**, *23*, 464-470.
48. Eyring, H., Viscosity, plasticity, and diffusion as examples of absolute reaction rates. *J Chem Phys* **1936**, *4*, 283-291.
49. Van Velzen, D.; Cardozo, R. L.; Langenkamp, H., A liquid viscosity-temperature-chemical constitution relation for organic compounds. *Ind Eng Chem Res* **1972**, *11*, 20-25.

50. Sastri, S. R. S.; Rao, K. K., A new temperature–thermal conductivity relationship for predicting saturated liquid thermal conductivity. *Chem Eng J* **1999**, *74*, 161-169.
51. Joback, K. G.; Reid, R. C., Estimation of pure-component properties from group-contributions. *Chem Eng Commun* **1987**, *57*, 233-243.
52. Ceriani, R.; Gonçalves, C. B.; Rabelo, J.; Caruso, M.; Cunha, A. C.; Cavaleri, F. W.; Batista, E. A.; Meirelles, A. J., Group contribution model for predicting viscosity of fatty compounds. *J Chem Eng Data* **2007**, *52*, 965-972.
53. Rowane, A. J.; Mallepally, R. M.; Gupta, A.; Gavaises, M.; M^cHugh, M. A., High-temperature, high-pressure viscosities and densities of *n*-hexadecane, 2,2,4,4,6,8,8-heptamethylnonane, and squalane measured using a universal calibration for a rolling ball-viscometer/densimeter. *Ind Eng Chem Res* **2019**, *58*, 4303-4316.
54. Dzidic, I.; Petersen, H. A.; Wadsworth, P. A.; Hart, H. V., Townsend discharge nitric oxide chemical ionization gas chromatography/mass spectrometry for hydrocarbon analysis of the middle distillates. *Anal Chem* **1992**, *64*, 2227-2232.
55. Wadsworth, P. A.; Villalanti, D. C., Pinpoint hydrocarbon types new analytical method helps in processing clean fuels. *Process Technology* 1992.
56. Baled, H. O. Density and viscosity of hydrocarbons at extreme conditions associated with ultra-deep reservoirs-measurements and modeling. PhD Thesis, University of Pittsburgh, 2012.
57. Baled, H. O.; Tapriyal, D.; Morreale, B. D.; Soong, Y.; Gamwo, I. K.; Krukonis, V.; Bamgbade, B. A.; Wu, Y.; M^cHugh, M. A.; Burgess, W. A.; Enick, R. M., Exploratory characterization of a perfluoropolyether oil as a possible viscosity standard at deepwater production conditions of 533 K and 241 MPa. *Int J Thermophys* **2013**, *34*, 1845-1864.

58. Baled, H. O.; Xing, D.; Katz, H.; Tapriyal, D.; Gamwo, I. K.; Soong, Y.; Bamgbade, B. A.; Wu, Y.; Liu, K.; M^cHugh, M. A.; Enick, R. M., Viscosity of *n*-hexadecane, *n*-octadecane and *n*-eicosane at pressures up to 243 MPa and temperatures up to 534 K. *J Chem Thermodyn* **2014**, 72, 108-116.
59. Rowane, A. J.; Mallepally, R. M.; Bamgbade, B. A.; Newkirk, M. S.; Baled, H. O.; Burgess, W. A.; Gamwo, I. K.; Tapriyal, D.; Enick, R. M.; M^cHugh, M. A., High-temperature, high-pressure viscosities and densities of toluene. *J Chem Thermodyn* **2017**, 115, 34-46.
60. Liu, K.; Wu, Y.; M^cHugh, M. A.; Baled, H.; Enick, R. M.; Morreale, B. D., Equation of state modeling of high-pressure, high-temperature hydrocarbon density data. *J Supercrit Fluids* **2010**, 55, 701-711.
61. Wu, Y.; Bamgbade, B.; Liu, K.; M^cHugh, M. A.; Baled, H.; Enick, R. M.; Burgess, W. A.; Tapriyal, D.; Morreale, B. D., Experimental measurements and equation of state modeling of liquid densities for long-chain *n*-alkanes at pressures to 265 MPa and temperatures to 523 K. *Fluid Phase Equil* **2011**, 311, 17-24.
62. Seiji Sawamura, T. Y. In *Rolling-Ball viscometer for studying water and aqueous solutions under high pressure* 14th International Conference on the Properties of Water and Steam, Kyoto, 2004; Kyoto, 2004; pp 429-434.
63. Kermis, T. W.; Li, D.; Guney-Altay, O.; Park, I.-H.; van Zanten, J. H.; M^cHugh, M. A., High-pressure dynamic light scattering of poly(ethylene-co-1-butene) in ethane, propane, butane, and pentane at 130 °C and kilobar pressures. **2004**, 37, 9123-9131.

64. ASTM International, Standard test method for dynamic viscosity and density of liquids by stabinger viscometer (and the calculation of kinematic viscosity). In Conshshocken, PA, USA, 2016.
65. JCGM, *Evaluation of measurement data — Guide to the expression of uncertainty in measurement (JCGM 100:2008)*. BIPM: 2008.
66. Special Metals: Inconel 718. http://www.specialmetals.com/assets/smc/documents/inconel_alloy_718.pdf (11/12/2018),
67. Caudwell, D. R.; Trusler, J. P. M.; Vesovic, V.; Wakeham, W. A., Viscosity and density of five hydrocarbon liquids at pressures up to 200 MPa and temperatures up to 473 K. *J Chem Eng Data* **2010**, 55, 5396-5396.
68. Eduljee, H. E.; Newitt, D. M.; Weale, K. E., Pressure-volume-temperature relations in liquids and liquid mixtures. Part I. The compression of *n*-hexane, *n*-heptane, *n*-octane, and of their binary and ternary mixtures, up to 5000 atmospheres. *J Chem Soc* **1951**, 0, 3086-3091.
69. Cutler, W. G.; McMickle, R. H.; Webb, W.; Schiessler, R. W., Study of the compressions of several high molecular weight hydrocarbons. *J Chem Phys* **1958**, 29, 727.
70. Kashiwagi, H.; Makita, T., Viscosity of twelve hydrocarbon liquids in the temperature range 298–348 K at pressures up to 110 MPa. *Int J Thermophys* **1982**, 3, 289-305.
71. Assael, M. J.; Papadaki, M.; Wakeham, W. A., Measurements of the viscosity of benzene, toluene, and *m*-xylene at pressure up to 80 MPa. *Int J Thermophys* **1991**, 12, 449-457.
72. Vieira dos Santos, F. J.; de Castro, C. A. N., Viscosity of toluene and benzene under high pressure. *Int J Thermophys* **1997**, 18, 367-378.

73. M^cHugh, M. A.; Krukonis, V., *Supercritical Fluid Extraction*. 2nd Edition ed.; Butterworth-Heinemann: 2013; p 608.
74. Burgess, W. A.; Tapriyal, D.; Gamwo, I. K.; Wu, Y.; M^cHugh, M. A.; Enick, R. M., New group-contribution parameters for the calculation of PC-SAFT parameters for use at pressures to 276 MPa and temperatures to 533 K. *Ind Eng Chem Res* **2014**, 53, 2520-2528.
75. Rosenfeld, Y., Relation between the transport coefficients and the internal entropy of simple systems. *Phys Rev A* **1977**, 15, 2545.
76. Novak, L., Self-diffusion coefficient and viscosity in fluids. *Int J Chem React Eng* **2011**, 9.
77. Novak, L., Fluid viscosity-residual entropy correlation. *Int J Chem React Eng* **2011**, 9.
78. Sauer, E.; Stavrou, M.; Gross, J., Comparison between a homo- and a heterosegmented group contribution approach based on the perturbed-chain polar statistical associating fluid theory equation of state. *Int J Chem Res* **2014**, 53, 14854-14864.
79. Allal, A.; Boned, C.; Baylaucq, A., Free-volume viscosity model for fluids in the dense and gaseous states. *Phys Rev E* **2001**, 64, 011203.